

Study of the Microstructure of the Gas Turbine Internal Blade

by

Nurul Najat bt Ahmad

Dissertation submitted in partial fulfilment of  
the requirements for the  
Bachelor of Engineering (Hons)  
(Mechanical Engineering)

SEPT 2011

Universiti Teknologi PETRONAS  
Bandar Seri Iskandar  
31750 Tronoh  
Perak Darul Ridzuan

**CERTIFICATION OF APPROVAL**

**Study of the Microstructure of the Gas Turbine Internal Blade**

by

Nurul Najat binti Ahmad

A project dissertation submitted to the  
Mechanical Engineering Programme  
Universiti Teknologi PETRONAS  
in partial fulfilment of the requirement for the  
BACHELOR OF ENGINEERING (Hons)  
(MECHANICAL ENGINEERING)

Approved by,

---

(Ir. Idris b Ibrahim)

UNIVERSITI TEKNOLOGI PETRONAS

TRONOH, PERAK

September 2011

## **CERTIFICATION OF ORIGINALITY**

This is to certify that I am responsible for the work submitted in this project, that the original work is my own except as specified in the references and acknowledgements, and that the original work contained herein have not been undertaken or done by unspecified sources or persons.

---

NURUL NAJAT BINTI AHMAD

## **ACKNOWLEDGEMENT**

Alhamdulillah Praise to Allah, the Most Gracious, Most Mercy, Most Wise for His Blessings, giving me the opportunity to still live in this world and oblige my duties as a Muslim. Blessings by Allah S.W.T to Prophet Muhammad (peace be upon him) for his sacrifices in his duty, spreading knowledge in the name of Allah S.W.T and teaching us the beauty of Islam.

First of all, I would like to express my feel of gratitude to the Almighty Allah S.W.T as His permission allows me to complete this task successfully. This dissertation is prepared due to the requirement for the Bachelor Of Engineering (Hons) (Mechanical Engineering). I would like to thank to my supervisor, Ir Idris bin Ibrahim for giving me the knowledge and guidance through all the process of completing this report.

Next I would like to thanks the lab technicians for helping me with the equipments needed for this project. Then, I would like to thanks my friends who have provided me with numerous comments and suggestions. I also like to thank Mr Shahrizal, Mechanical Executive from PETRONAS Carigali Sdn Bhd, for his knowledge and information of gas turbine in the plant. Last but not least, I would like to thank my beloved parents, Tn Hj Ahmad bin Ishak and Pn Hj Masitah bt Mansor for their never ending support that helps me completed the project. Thank you.

## ABSTRACT

High Pressure Turbine (HPT) first stage blade is the most important rotational components of aero-engine. It operates at high temperature and under conditions of extreme environmental attack such as oxidation and corrosion, is especially subjected to degradation by oxidation, corrosion and wear. Due to the elevated temperature been introduced on the turbine blades, they faced several failure such as thermal stress failure and creep. This failure is very common and always occurred on this life limiting component of gas turbine. Further study on the microstructure behavior with respect to the temperature along the blade is carried out to predict the cycle life of the blade.

The objective of this project is basically to study on the microstructure of Nickel based Superalloy characterization. The study is mainly focusing on the evaluation of the morphology change of the  $\gamma'$  particles, carbide precipitation and characterization of particle type and size. Then, a complete procedure and testing related with the study of gas turbine blades were performed using relevant equipment and tools. The procedure involves preparing metallographic sample, chemical analysis and analyzing the microstructure under FESEM and EDS. Though, the main objective of this project is to create a complete profile of microstructure along the turbine blade. This profile is believed to be very useful in the industry to predict the cycle life of turbine blade.

Thorough analysis been done, the microstructure undergoes transformations which likely degrade the mechanical properties of the alloy, including  $\gamma'$  coarsening, increased carbide precipitation in grain boundaries, and increasing grain size with respect to temperature. From the analysis, we can predict the temperature profile alongside the blade, which is increase from lower part to upper part. Therefore, the operating temperature of gas turbine need to be maintain so that the microstructure of blade is not affected and as well reduce the lifespan of turbine blade.

## TABLE OF CONTENTS

<b>CERTIFICATION OF APPROVAL</b>		ii
<b>CERTIFICATION OF ORIGINALITY</b>		iii
<b>ACKNOWLEDGEMENT</b>		iv
<b>ABSTRACT</b>		v
<b>TABLE OF CONTENTS</b>		vi
<b>LIST OF FIGURES</b>		viii
<b>LIST OF TABLES</b>		viii
<b>CHAPTER 1:</b>	<b>INTRODUCTION</b>	1
	1.1 Project Background	2
	1.2 Problem Statement	2
	1.3 Objectives & Scope of Study	2
	1.4 Relevancy & Feasibility of the Project	3
<b>CHAPTER 2:</b>	<b>LITERATURE REVIEW</b>	4
	2.2 Critical Analysis of Literature	4
	2.2 List of References	9
<b>CHAPTER 3:</b>	<b>METHODOLOGY</b>	12
	3.1 Research Methodology	12
	3.2 Project Activities	13
<b>CHAPTER 4:</b>	<b>RESULT &amp; DISCUSSION</b>	21
	4.1 Background Information	21
	4.2 Turbine Blade Section	22
	4.3 Chemical Analysis	24
	4.4 Microstructure Analysis	26
	4.5 Hardness Testing	37

<b>CHAPTER 5:</b>	<b>CONCLUSION &amp; RECOMMENDATION.</b>	.	39
<b>REFERENCES</b>	.	.	40
<b>APPENDIX</b>	.	.	42

## LIST OF TABLES

TABLE 3.1:	Contemporary procedure for Ni-Based Superalloy	19
TABLE 3.2:	Basic etchants for Ni and alloy	20
TABLE 4.1:	Material composition for each sample	26
TABLE 4.2:	Average particle diameter for each sample	28
TABLE 4.3:	Temperature estimation from particle size of gas Turbine Blade	31
TABLE 4.4:	Hardness value for each sample	37

## LIST OF FIGURE

FIGURE 1.1:	Turbine blade 1 <sup>st</sup> stage	2
FIGURE 2.1:	Microstructure of Alloy 718	8
FIGURE 2.2:	Fluid flow temperature distribution around the first stage blades	9
FIGURE 2.3:	The micrograph that shows the location where the crack started	10
FIGURE 2.4:	Continuous band of grain boundary carbides & $\gamma'$ morphology in the hottest zone.	11
FIGURE 2.5:	Gamma prime $\gamma'$ morphology in the zone 3	11
FIGURE 3.1:	The flowchart of the project methodology and its descriptions	12
FIGURE 3.2:	Electrical Discharge Machining (EDM)	15
FIGURE 3.3:	Equipment used for hot mounting	16
FIGURE 3.4:	Hot mounting procedure	16
FIGURE 3.5:	Silicon grid paper	17
FIGURE 3.6:	Grind the specimen at 90 degrees	18
FIGURE 3.7:	Metadi fluid and diamond paste for polishing	19
FIGURE 3.8:	Optical Microscope	20
FIGURE 3.9:	FESEM	21
FIGURE 3.9:	Microhardness Testing Machine	22
FIGURE 4.1:	ROLLS-ROYCE ALLISON 501-KB7 Gas Generator	23
FIGURE 4.2:	Temperature distribution of blade	24
FIGURE 4.3:	Sections for each stage of turbine blade	25
FIGURE 4.4:	Chemical composition for sample M2	27

FIGURE 4.5: The relationship between mechanical properties and gamma prime particle size	29
FIGURE 4.6: The relationship between grain size and temperature when strain rate is $0.01 \text{ s}^{-1}$ , holding time is 30 min.	30
FIGURE 4.7: Relationship of particle size of gas turbine blade and temperature	31
FIGURE 4.8: Temperature and particle size relationship on the blade arrangement	32
FIGURE 4.9: $\gamma'$ morphology for first stage blade	33
FIGURE 4.10: $\gamma'$ morphology for second stage blade	35
FIGURE 4.11: $\gamma'$ morphology for third stage blade	37

# CHAPTER 1

## INTRODUCTION

### 1.1 Project Background

Gas turbine is a form of heat engine where a hot pressurized gas, produced by combustion of fuel and air, spin the turbine. The ignition of fuel and air results in rapid expansion of gas which causes high speed rotation as the hot pressurized gases flow across aerodynamically shaped turbine blade. A turbine blade is the limiting component of gas turbine and responsible for extracting energy from the high temperature and high pressure gas produced by the combustor.

The blade is subjected to forces in the three directions which are the rotor driving force along the radial direction, axial forces caused by the gas flow and forces acting normal to the turbine shaft due to the centrifugal forces. The blade is also faced a differential thermal stresses, erosion-corrosion, high stresses, and a potentially high vibration environment that can obstruct its smooth functioning.

Turbine blades always faced higher entry temperatures to maintain and increase the power to weight ratio and as well improve the efficiency of gas turbine. Thus, the material of turbine blades must withstand the high operating temperature been introduced from the combustor section. The turbine blades must also endure the varying temperature and should have structural stability when exposed to varying temperature. However, the turbine blade which is the life limiting component of gas turbine needs to face several failures such as thermal fatigue, oxidation or corrosion and creep.

Many researches had been done to overcome the problem of high temperature and one of them is the selection of a new material that capable of operating at high temperatures. Generally, turbine blades made from various type of material such as steels, titanium alloys and nickel base alloys. To hold up the high temperature of gas

turbine, a system called blade cooling has been introduced. This system maintains the temperature of blade at a value low enough to preserve the desired material properties. Blade cooling may be classified based on cooling site which are external cooling and internal cooling. Cooling medium can be liquid cooling or air cooling.

## 1.2 Problem Statement

Turbine blades (see Figure 1.1) are exposed to high temperature gas exiting the combustion chamber to produce mechanical work. They are also cooled down by the compressor air which flows through the blade internal passage forming an air film between the blade and the hot gas. Often the turbine blade will suffer from thermal stress failure as well as failure due to creep. Thus, it is importance if study of the turbine blade microstructure can be conducted to understand its profile with regard to the gas turbine operating temperature.



*Figure 1.1: Turbine blade 1<sup>st</sup> stage.*

## 1.3 Objective and Scope of Study

### 1. Study on the microstructure of Nickel based Superalloy characterization

A complete study on turbine blade profile & microstructure behavior with regard to the previous research has been done by reading related journals and books. The study is mainly focusing on the evaluation of the morphology change of the  $\gamma'$  particles and characterization of particle type and size. The microstructure result obtained from the turbine blade will be analyzed according to the mechanical damage they have been experienced such as creep.

2. Analysis the microstructure characteristic of the turbine blade by using appropriate procedure and equipments.

A suitable methodology has been developed to investigate the microstructure of the turbine blade for example sample preparation procedure, microstructures analysis procedure and also hardness test. To perform the study, appropriate equipments were chose. These equipments were chosen based on their function and also their availability in UTP. Mostly, Field Emission Scanning Electron Microscope (FESEM) will be used to investigate the microstructure of the blade. Hardness Testing Machine will also be used to study the hardness of the material with respect to the temperature.

3. Establish profile of microstructure vs. temperature of turbine blades.

After collecting all the data required, a study on microstructure pattern will be carry on. Then, the pattern will be identified according to the specific zones on the blade. The result obtain will be compared with the previous result from previous researches. ANSYS result will be used to compare the temperature distribution along the blade and as well describing the microstructure pattern.

#### **1.4 Relevancy and Feasibility of the Project**

Researches on evaluating the thermomechanical behavior for turbine blade materials that are made up of Ni base superalloys have garnered increased interest in recent years. Study on the turbine blade microstructure profile with regard to the gas turbine operating temperature can help to understand and predict the cycle life of the turbine blade. By performing this project, a microstructure catalogue or profile can be generated along the turbine blade. The catalogue can be an important references in the future for predicting and maintaining the cycle life of the turbine blade been used in the industry. This project is feasible to be done for final year project within 2 semesters since all the equipments and tools needed are provided inside UTP. This project also has sufficient references to be referred.

## **CHAPTER 2**

### **LITERATURE REVIEW**

#### **2.1 Critical Analysis of Literature**

##### **2.1.1 Turbine Blade**

Turbine blades are generally considered to exhibit a high level of reliability, and failure rates are considered low. High Pressure Turbine (HPT) first stage blade is the most important rotational components of aero-engine [1]. It operates at high temperature and under conditions of extreme environmental attack. (Harrison & Henderson, 2000) said turbine blade materials need to have a balance of key properties to meet the operational parameters [2]. They must have high stiffness and tensile strength to ensure accurate blade location and resistance to overspeed burst, high fatigue strength and crack propagation resistance, high creep strength to avoid distortion and growth and also oxidation and corrosion resistance and resistance to fretting damage at mechanical fitting. The most common material is the nickel-based 'super-alloy' materials that can withstand a very aggressive environment of high temperature and high stress within the hot gas path of a turbine engine.

According to (Carter, 2004)

Nickel is considered as a most suitable basis for alloying since it exhibits, by virtue of its almost-full third electron shell, a high capacity for forming stable alloys without phase instability. It also forms, with chromium additions, Cr<sub>2</sub>O<sub>3</sub>-rich surface oxide films, which are both stable and protective, restricting movement of both metallic elements in the outward direction, and aggressive atmospheric elements such as oxygen, nitrogen and sulphur in an inward direction. Nickel will also form, with aluminium additions, Al<sub>2</sub>O<sub>3</sub> surface layers, which are highly oxidation-resistant at very high

temperatures. Nickel-base alloy turbine blade materials are immensely complicated in terms of microstructure, with the efforts of alloy developers over the years having created a range of fine precipitates which confer high levels of resistance to creep.[3]

Blade failures can be caused by a number of mechanisms under the turbine operating conditions of high rotational speed at elevated temperatures. Generally, blade failures can be grouped into two categories: (a) fatigue, including both high and low cycle fatigue (b) creep rupture [4]. However, under normal conditions, blades should never be operated at excessive temperatures for long enough periods to cause microstructural damage. Some elevated temperature exposure is permitted for very limited periods, for example during start or for emergency situations. Such exposure should be strictly controlled, with inspection for possible damage, including metallographic examination of sample blades, being required. Once the microstructure has been degraded by exposure to elevated temperature, it is normally assumed that the blades have been damaged and replacement is mandatory [3].

Inconel 718 as shown in Figure 2.1 is a high-temperature alloy with about 53% nickel, is the most common nickel-based material in use. More than half of the hot end of a jet engine is made from this material [5]. The specimen is a non-rotating grade with a fine grain size and considerable delta phase and large MC-type. The microstructure of Inconel 718 is shown as below [6]:

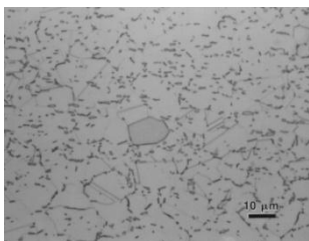


*Figure 2.1a*

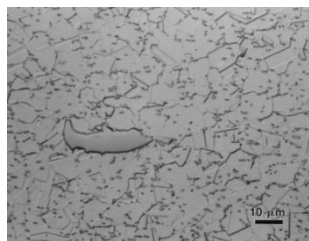


*Figure 2.1b*

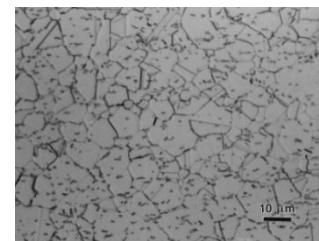


*Figure 2.1c*

*Figure 2.1: Microstructure of Alloy 718 (nonrotating grade) with a fine grain size, considerable delta and large primary MC carbides revealed using a) glyceric acid, b) the “15-10-10” etch and c) the Lucas reagent.*

### 2.1.2 Experimental Procedure

To perform the experiment as according to (Vardar & Ekerim, 2006), examination of the blade material was made for two different zones of the blade: near the cracked bladetip and close to the blade platform [7]. Later, a standard metallurgical procedure was done by preparing the samples, polished by standard techniques and etched with solution of 20 ml HNO<sub>3</sub> and 60 ml HCl. The investigation then followed by experimental tests, including optical microscopy, SEM, EDS, (XRD) and X-Ray fluorescence (XRF). Similar methodology was involved in the analysis of superalloy turbine blade after 600 h service [8]. Two blades have been used. Blade A remained intact for investigation of top tip surface and Blade B was sectioned for investigation; section contains all visible cracks on the pressure side was taken longitudinally from blade B using EDM cutting. The section then was polished and microstructure was revealed with an electrochemical etching method in an etching agent of 10% oxalic acid under 6 V DC for 20–30 s.

From these researches, an improved procedure or methodology can be perform in the study of microstructure of turbine blade. First, the blade will be sectioning to several samples. The author had received specimens from PETRONAS Carigali Sdn Bhd which came from different stages of turbine engine. Examination of the blade will be made at different zones of blade: near the cracked bladetips and close to the blade platform [7]. To improve the methodology, additional zones; middle blade will be examined to get a complete profile of microstructure along blade with respect to temperature. The microstructure profile will be compare with the existing fluid flow temperature distribution as shown is Figure 2.2 [4].

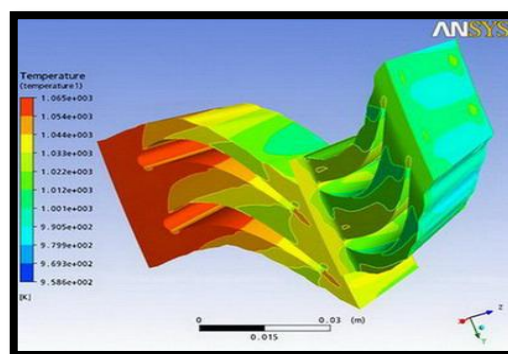
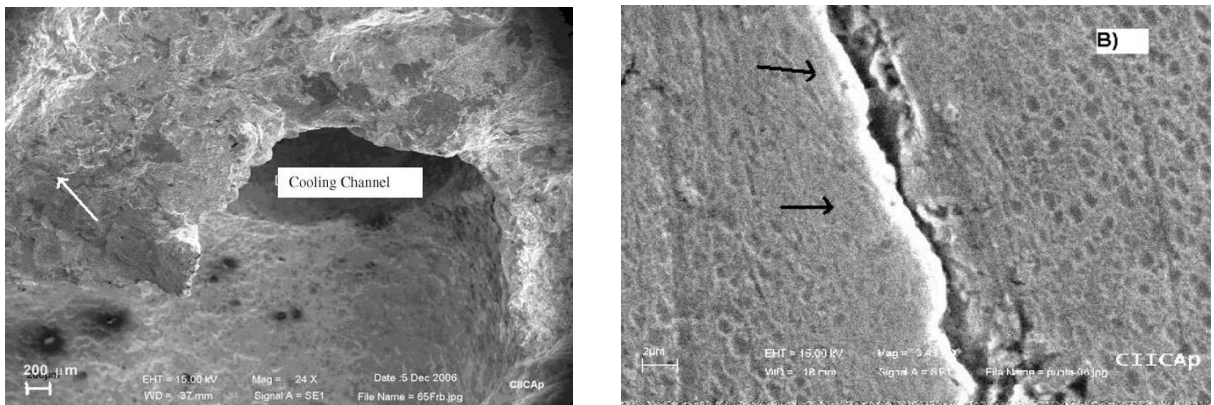


Figure 2.2: Fluid flow temperature distribution around the first stage blades.

From the analysis been done, several result were found indicated the existence of failure to the blade especially due to creep and thermal stress failure. On one study of failure analysis (Kubiak, et al., 2009), two cracks were identified in this blade as shown in Figure 2.3; one from the securing pin hole up to the blade base and the second one in the leading edge of the blade body, exactly at 1.5 cm from the blade base [ix]. This microstructure is hard and brittle, and leads to failures. A micro hardness profile along the blade also indicates that in the fractured zone, martensite was observed and increase of hardness was present. Carbides were also distributed in discrete form and gamma prime phase appears in the form of circle/cubic with a size between 0.5 and 1  $\mu\text{m}$ , whereas the carbides, along the grain boundaries, were 10  $\mu\text{m}$  long and the grains are nearly 100 $\mu\text{m}$  in length.



*Figure 2.3: The micrograph that shows the location where the crack started.*

Meanwhile in one report of failure analysis (Mazur, Luna-Ramirez, Juarez-Islas, & Campos-Amezcu, 2004), the microstructure evaluation of different zones of the blade shown in was carried out. The microstructure of the blade hot section (airfoil) was compared to the cold reference zone (blade root) to evaluate the degree of alloy deterioration. Based on Figure 2.5 and Figure 2.5, the comparative evaluation includes the morphology change of the  $\gamma'$  particles, carbide precipitation and characterization of grain type and size [x].

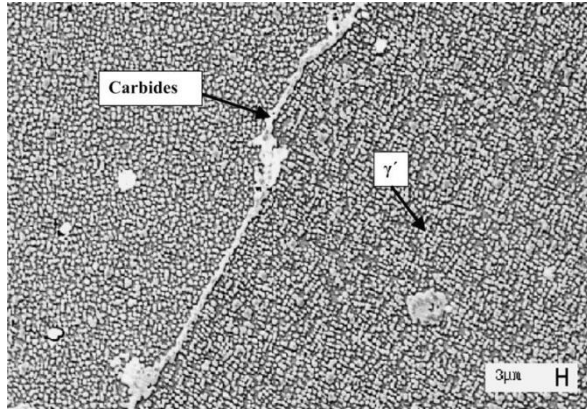


*Figure 2.4: Continuous band of grain boundary carbides and  $\gamma'$  morphology in the hottest zone.*

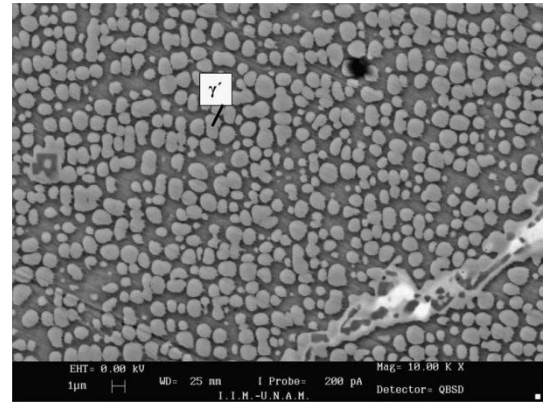


*Figure 2.5: Gamma prime  $\gamma'$  morphology in the middle zone.*

From the result achieved by the previous researches, the author can perform the analysis of the Ni based Superalloy microstructure. After preparing the metallographic specimens and view under optical microscope and scanning electron microscope (SEM), the microstructure viewed can be analyze by comparing the result with the previous result found in the relevant journal. The result will be interpreted according to morphology change of the  $\gamma'$  particles and characterization of particle type and size. And then, a complete profile of microstructure with respect to blade profile will be generated. The blade provided is divided into 3 zones (upper, middle and lower).

## 2.2 List of References

No	Title	Objective	Methodology	Result
1.	Failure Analysis of Gas Turbine Blades: Mehdi Tofighi Naeem, Seyed Ali Jazayeri, Nesa Rezamahdi (2008)	Evaluate the creep-fatigue properties of the first and second stage blades under cycling duty by performing a complete metallurgical investigation and mechanical analysis.	<ol style="list-style-type: none"> <li>Using ANSYS Workbench 11.0 software (advanced CFD section) to form a steady state gas flow</li> <li>The metallurgical investigation used visual examination, photographic documentation, NDT, optical microscopy, SEM and EDS</li> <li>Prepared several longitudinal and transverse sections from the blades. These specimens were polished by standard techniques and were etched by solution of 5ml 4 CuSO, 50mlH<sub>2</sub>O, and 50ml HCl.</li> </ol>	<ol style="list-style-type: none"> <li>Micro-cavities were found on fracture surfaces</li> <li>Carbides precipitation in grain boundaries (formation of continuous films and dispersed particles of carbides)</li> <li>Degradation of the alloy <math>\gamma</math> phase (irregular growing of <math>\gamma'</math> particles).</li> <li>Many annealing twins were observed at different regions.</li> <li>Mechanical analysis: temperature and pressure contours and the magnitude and direction of flow velocity showed consistency with real conditions.</li> </ol>
2.	Analysis of superalloy turbine blade tip cracking during service: Yu-jiang Xie, Mao-cai Wang Ge Zhang, Min Chang (2005)	Investigate the blades with premature tip cracks and improve the safety of the aircraft and the overhaul and refurbishment practice.	<ol style="list-style-type: none"> <li>The evaluation was carried out after 600 h service.</li> <li>2 blades been used: Blade A remained intact for investigation of top tip surface and Blade B was sectioned for investigation; section contains all visible cracks on the pressure side was taken longitudinally from blade B using EDM cutting.</li> <li>The section was polished and microstructure was revealed with an electrochemical etching method in an etching agent of 10% oxalic acid under 6</li> </ol>	<ol style="list-style-type: none"> <li>Blade tip top surface examination <ul style="list-style-type: none"> <li>many gray–white strips on the top surface of squealer tip indicated that turbine blades were exposed to corrosive conditions</li> </ul> </li> <li>Blade tip with crack section analysis <ul style="list-style-type: none"> <li>all cracks look like lines axially, indicating that cracks grow transgranularly. Corrosion products can be seen in the crack in form of grains and flakes</li> <li>EDS analysis results show that the corrosion products are mainly oxide and carbide; pieces of Al<sub>2</sub>O<sub>3</sub> are identified in the crack.</li> <li>many corrosion pits can be found on the</li> </ul> </li> </ol>

			V DC for 20–30 s. 4. MEF-4 A Optical Microscope and Philips XL400-FEG SEM equipped with EDS were used to observe the microstructure and analyze the chemical composition of local regions.	blade tip region top surface
3.	Creep-fatigue failure of an aero engine turbine blades: I. Salam, A. Tauqir, A.Q. Khan (2001)	Components of the turbine region (turbine blades of the 1st and 2nd stages) were examined subjected to metallurgical investigation to delineate the cause of failure.	1. Samples were cut from different locations and prepared for optical and scanning electron microscopy. 2. Etching was performed in gliceragia and then in 2% H2SO4 in water 3. The fracture surfaces were examined with a scanning electron microscope (SEM). 4. Chemical composition was determined with the help of energy dispersive spectrometry (EDS) and C/S analyzer. 5. Grain size was measured using an image analyzer attached with the optical microscope. 6. Hardness was measured by using Vicker's hardness testing machine.	Fractured Blades 1. Visual examination: two clear regions-a shiny region, 50% of the total fracture area and a dark black area covering the other 50% of the fractured surface. 2. Microstructure: EDS analysis shows high concentration of Ti and Mo in these particles. Twinning is also clear in some of the grains and fine carbides are also present along the grain boundaries. 3. Fractography: fatigue crack start from surface cracks while multiple origins are present. Intergranular fracture is clear at the origins. 4. Result from hardness test, grain size and chemical composition are also presented in the report.
6.	Failure analysis of the 150MW gas turbine blades J. Kubiak, G.	Find out the main cause of the blades failure.	1. Metallurgical examination to establish the metallurgical mode of failure _ Take several specimens to examine a microstructure in three different parts of the blades.	1. Two cracks were identified in this blade; one from the securing pin hole up to the blade base and the second one in the leading edge of the blade body, exactly at 1.5 cm from the blade base

	Urquiza, J.A. Rodríguez, G. González, I. Rosales, G. Castillo, J. Nebradt (2008)		<p>1. Expose the cracks to the fractography of the cracked blades and determine the metallurgical mode of the failure.</p> <p>2. Micrography and fractography of the blade a set of micrographs obtained through scanning electronic microscopy (SEM).</p> <p>3. Microstructure examination of the blade material. The microstructure of the blade metal was examined in four zones: at the root of the blade, the hub, in the mid span and in the tip of the blade.</p>	<p>2. This microstructure is hard and brittle, and leads to failures. A micro hardness profile along the blade, indicates that, in the fractured zone, where this martensite was observed an increase in the hardness was present</p> <p>3. Carbides were distributed in discrete form and gamma prime phase appears in the form of circle/cubic with a size between 0.5 and 1 <math>\mu\text{m}</math>, whereas the carbides, along the grain boundaries, were 10 <math>\mu\text{m}</math> long and the grains are nearly 100 <math>\mu\text{m}</math> in length.</p>
7.	Metallographic Techniques For Superalloys George F. Vander Voort, Elena P. Manilova, Gabriel M. Lucas	Presents the use of new metallographic materials to prepare these alloys with emphasis on modern, four- and five-step practices.	<p>Mounting: Compression-mounting thermosetting epoxy resins, such as Epomet thermosetting resin, provide the best edge retention.</p> <p>Grinding: used 180- or 240-grit SiC paper or rigid grinding disk (RGD) and a coarse size diamond abrasive.</p> <p>Polishing: acidic alumina slurries and basic colloidal silica slurries have been employed for final polishing of superalloys.</p> <p>Ethching: Numerous etchants are used to reveal the structure of superalloys.</p>	<p>Cast Alloy: Metallographers are often requested to reveal the dendritic structure of cast specimens and perform measurements of the secondary dendrite arm spacing.</p> <p>Wrought alloys: evaluated for grain size and the presence of second-phase precipitates.</p>

## CHAPTER 3 METHODOLOGY

### 3.1 Research Methodology

Figure 3.1 below describes the method of conducting the project.

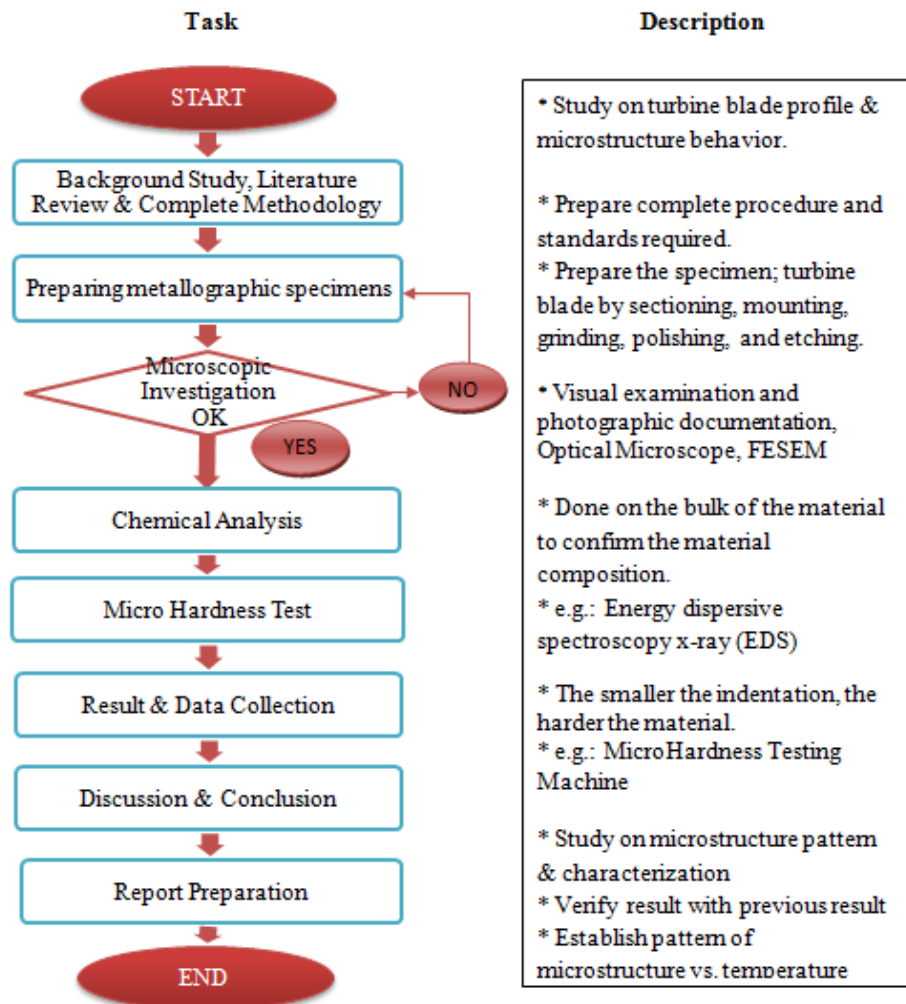


Figure 3.1: The flowchart of the project methodology and its description.

## 3.2 Project Activities

### 3.2.1 Sample Preparation: Sectioning

The first step in preparing a specimen for metallographic or microstructural analysis is to locate the area of interest. Sectioning or cutting is the most common technique for revealing the area of interest. Proper sectioning will produce flat and cut close to the area of interest and minimal microstructural damage.

In this experiment, EDM (Figure 3.2) was used to section the turbine blade into small specimens. Electric discharge machining (EDM) is a manufacturing process whereby a desired shape is obtained using electrical discharges (sparks). Material is removed from the workpiece by a series of rapidly recurring current discharges between two electrodes, separated by a dielectric liquid and subject to an electric voltage.



*Figure 3.2: Electrical Discharge Machining (EDM).*

The turbine blades were sectioned to 3 parts (1 cm x 1cm) for each blade. The samples were cut at lower part (D), middle (M) and upper part (U). First stage blade was exposed to higher temperature exposure from the hot gas than second and third blade.

### 3.2.2 Sample Preparation: Mounting

The specimen must be mounted and prepared for examination with a metallurgical microscope. Before mounting, all oil and grease should be removed from the sample by washing it in acetone or ethanol, then drying it. Using the equipment shown in Figure 3.3 hot mounting was performed with cylindrical shape (diameter: 30mm) mould.

#### Procedure for Hot Mounting

The purpose of mounting is to get the flat surface of sample so that it would be easier for grinding process to take place.



*Figure 3.3: Equipment used for hot mounting.*

The procedure for mounting is shown in the Figure 3.4 below:



*Figure 3.4a: The mounting is cleaned using release agent.*

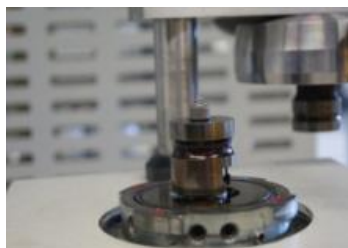


*Figure 3.4b: The sample was put on the top of the mounting.*



*Figure 3.4c: Phenolic powder was filled inside the mounting together with the sample.*



*Figure 3.4d: Once the setup has finished, it took about 10minutes for heating and cooling process.*



*Figure 3.4e: The mounted sample.*

### **3.2.3 Sample Preparation: Grinding**

Once the sample has been mounted, the resin block must be ground flat. Grinding process was performed by using Grinder and Polisher machine model Metaserv 2000. The samples were ground with SiC paper and running water and rotated the sample through  $90^\circ$ . The SiC paper (see Figure 3.5) used ranging from the coarsest grit paper, 60 grits to 1200 grits to eliminate the scratches from the previous grinding stage otherwise they will not be removed in polishing.



*Figure 3.5: Silicon grid paper 120 grit (left) and 1200 grit (right).*

The procedure for grinding is shown as below:

- (1) Open water line located behind grinder.
- (2) Starting on the 60 grit size, place prepared specimen, or metal face down of abrasive surface, and being sliding specimen against abrasive in a forward and backward motion.
- (3) Next, turn specimen 90 degrees and repeat above procedure on the 120 Grit surface.



*Figure 3.6: Grind the specimen at 90 degrees.*

- (4) Finally, turning specimen 90 degrees (Figure 3.6) and repeat procedure (3) now on the 320,400,600 and 1200 Grit surface.
- (5) Close water line.

#### **3.2.4 Sample Preparation: Polishing**

Polishing is used to create a flat, defect-free surface for examination of a metal's microstructure under a microscope. Grinder and Polisher machine model Metaserv 2000 was consist of rotating discs covered with soft cloth impregnated with diamond particles (1 micron size) and an oily lubricant.

The procedure of polishing is shown as below:

- (1) Providing a polishing pad having at least one circular groove wherein the circular groove encircles an axis of rotation of the polishing pad.
- (2) Apply metaDi fluid ( Figure 3.7) on the polishing pad;
- (3) Apply diamond paste on the polishing pad and specimens



Figure 3.7: metaDi Fluid (Left) and Diamond Paste (Right).

- (4) Rotating the polishing pad; and
- (5) Place a specimen on the polishing pad and polish specimen until we obtained mirror image.

Table 3.1 below show the standard load, speed and time for polishing and grinding procedure. In this experiment, trident cloth was used with 1-micron diamond paste [6].

Table 3.1: Contemporary Procedure for Ni-Based Superalloy.

Table 1. Contemporary Procedure for Ni-Based Superalloys				
Surface	Abrasive/Size	Load Lb (N)/ Specimen	Platen Speed (rpm)/Direction	Time (minutes)
Carbimet® waterproof discs (psa)	220-240 (P240-P280) grit SiC water cooled	6 (27)	240-300 Comp.	Until Plane
Ultra-Pol Silk Cloth (psa)	9- $\mu$ m Metadi® Supreme Diamond Suspension	6 (27)	100-150 Comp.	5
Trident cloth (psa)	3- $\mu$ m Metadi® Supreme Diamond Suspension	6 (27)	100-150 Comp.	4
Trident cloth (psa)	1- $\mu$ m Metadi® Supreme Diamond Suspension	6 (27)	100-150 Comp.	3
Microcloth pad (psa)	0.05- $\mu$ m Masterprep™ alumina slurry	6 (27)	80-150 Contra	2

### 3.2.5 Sample Preparation: Etching

Metallographic etching is a technique used to highlight features of metals at microscopic levels such as grain boundaries, phase differences and inclusions. To analyze planar features such as grain boundaries, a metallic sample must be polished to a very fine mirror-like finish. Under a microscope, such a finely polished surface just looks like a plain white field therefore to create contrast between the elements of

the metal's microstructure, chemical solutions known as etchants are used to selectively corrode some of those elements, which show up as darker regions.

Marble reagent (see Table 3.2) was used to reveals the grain structure of superalloy. This reagent was swab on the sample for 30 seconds and then washed by water and methanol to avoid over etching.

*Table 3.2: Basic etchants for Ni and Alloy.*

Nickel and Alloys	
Composition	Comments
48. 5 g FeCl <sub>3</sub> 2 mL HCl 99 mL ethanol	Carapella's etch for Ni and Ni-Cu (Monel) alloys. Use by immersion or swabbing.
49. 40-80 mL ethanol 40 mL HCl 2 g CuCl <sub>2</sub>	Kalling's no.2 etch ("waterless" Kalling's) for Ni-Cu alloys and superalloys. Immerse or swab specimen up to a few minutes.
50. 50 mL water 50 mL HCl 10 g CuSO <sub>4</sub>	Marble's reagent for Ni, Ni-Cu, and Ni-Fe alloys and superalloys. Immerse or swab sample 5-60 seconds. Reveals grain structure of superalloys.
51. 15 mL HCl 10 mL glycerol 5 mL HNO <sub>3</sub>	"Glyceregia", for superalloys and Ni-Cr alloys. Swab specimen for 5-60 seconds. Mix fresh. Do not store. Use under a hood.
52. 60 mL glycerol 50 mL HCl 10 mL HNO <sub>3</sub>	Modified Glyceregia for superalloys. Reveals precipitates. Use under hood; do not store. Add HNO <sub>3</sub> last. Discard when dark yellow. Immerse or swab specimen 10-60 seconds.

### 3.2.6 Microstructure Examination

- Optical Microscope

The optical microscope (Figure 3.8) uses visible light and a system of lenses to magnify images of small samples. The actual power or magnification of a compound optical microscope is the product of the powers of the ocular (eyepiece) and the objective lens. The magnification employed during the experiment were 50x and 100x.



*Figure 3.8: Optical Microscope.*

One big advantage of light microscopes is the ability to observe living cells. It is possible to observe a wide range of biological activity, such as the uptake of food, cell division and movement.

- Field Emission Scanning Electron Microscope (FESEM)



*Figure 3.9: FESEM*

FESEM (Figure 3.9) with ultra high resolution imaging is used to analyze up to nano scale surface structure and morphology of solids. EDS is embedded in this equipment to identify the different elements present in the specimen. Functions of FESEM are to analyze surface morphology and topography, point to point elemental analysis, line scan analysis and x-ray mapping. The microstructure analysis was conducted using Carl Zeiss AG with magnification up to 10K X, 5K X and 1K X with a working distance 8.0mm.

### **3.2.7 Chemical Analysis - EDS**

Energy-dispersive X-ray spectroscopy (EDS) is a chemical microanalysis technique used in conjunction with scanning electron microscopy (FESEM). The EDS technique detects x-rays emitted from the sample during bombardment by an electron beam to characterize the elemental composition of the analyzed volume. Features or phases as small as 1  $\mu\text{m}$  or less can be analyzed. EDS result can be analyzed quantitatively and qualitatively.

### 3.2.8 Hardness Test

Then hardness of the sample was measured by conducted Micro hardness testing using Leco LM 247 AT, microhardness machine (see Figure 3.10). The unit of hardness used was Vickers Pyramid Number. The load used was 1000gf with the magnification of 50X.

The hardness reading for each sample was taken at three different locations of the sample's surface to get the accurate average hardness of the sample. These hardness values provided the data to estimate the yield strength properties of the Nickel based superalloy.



*Figure 3.10: Microhardness Testing Machine used for indentation test.*

## CHAPTER 4

### RESULT AND DISCUSSION

#### 4.1 Background Information

Gas turbines are extensively used for power generation and for the propulsion of aircraft and vessels. Rolls-Royce Allison 501-KB7 turbine unit (refer Figure 4.1) consist of four-stage rotor and vane assembly (stages 1, 2, 3, and 4). The 1st stage blades and vanes are air cooled. The rotor assembly absorbs the necessary energy from the expanding gases to drive the compressor rotor, the engine driven accessories, and the driven equipment through the PTO assembly. [11]

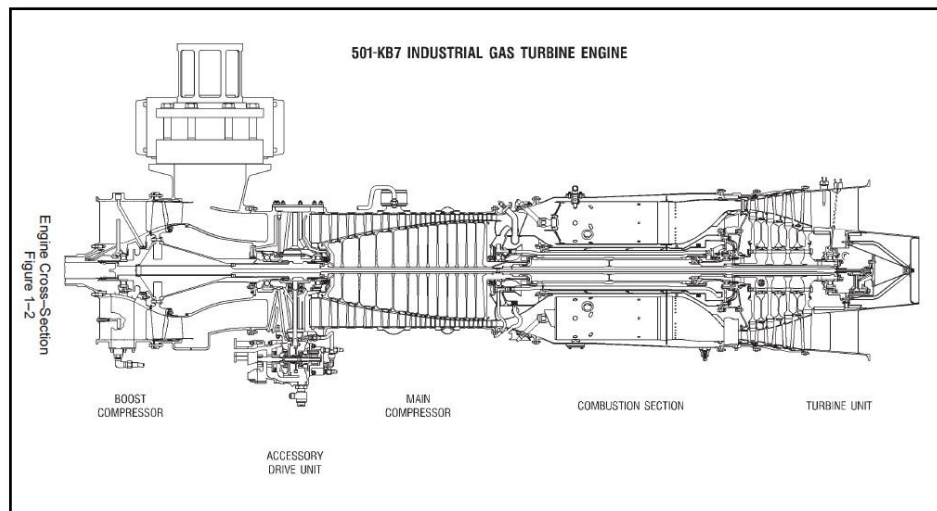


*Figure 4.1: Rolls-Royce Allison 501-KB7 Gas Generator.*

The hot gas temperature from combustor to first stage vane (control temp) is around 950 – 1057 °C depending at engine speed 14200 – 14600 rpm. The temperature is gradually dropped from 1<sup>st</sup> stage turbine to the 4<sup>th</sup> stage until exhaust. Warning temperature will be schedule if the control temperature reach 1093°C at 15400rpm and above. The turbine will tripped if the control temperature exceeds 1104 °C and

engine speed reach 15800 rpm. These entire maximum setting were established by Rolls Royce Corporation.

## 4.2 Turbine Blade Section

The maximum temperature experienced by the blade is along the leading edge, at about two-third of the blade height. Generally, the differential temperature along the leading edge during service results in a graded microstructure in the blade, and is a function of distance from the blade root platform [12]. The first stage turbine blade was introduced to maximum temperature (950°C -1057°C) and the temperature will gradually decreased along the blade as shown in Figure 4.2. Upper part of the blade has the maximum temperature meanwhile the temperature drop gradually until lower part of turbine blade. First stage blade was exposed to higher temperature exposure from the hot gas than second and third blade [13]. During high temperature service, the microstructure slowly degrades by a coarsening process. In the presence of stress, e.g. caused by the centrifugal load in a gas turbine blade, a severe directional coarsening, so-called rafting, of the initially cuboidal  $\gamma'$ -particles into a plate-like structure occurs.

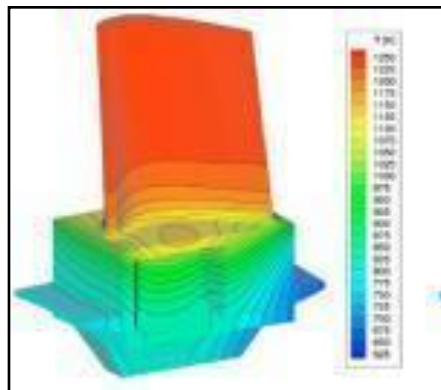


*Figure 4.2: Temperature distribution of blade without cooling channels.*

To study the correlation of material microstructure and creep exposure, the turbine blades were sectioned to 3 parts (1 cm x 1cm) for each blade (Figure 4.3). The samples were cut at lower part (D), middle (M) and upper part (U).



Figure 4.3a: Turbine Blade 1<sup>st</sup> Stage

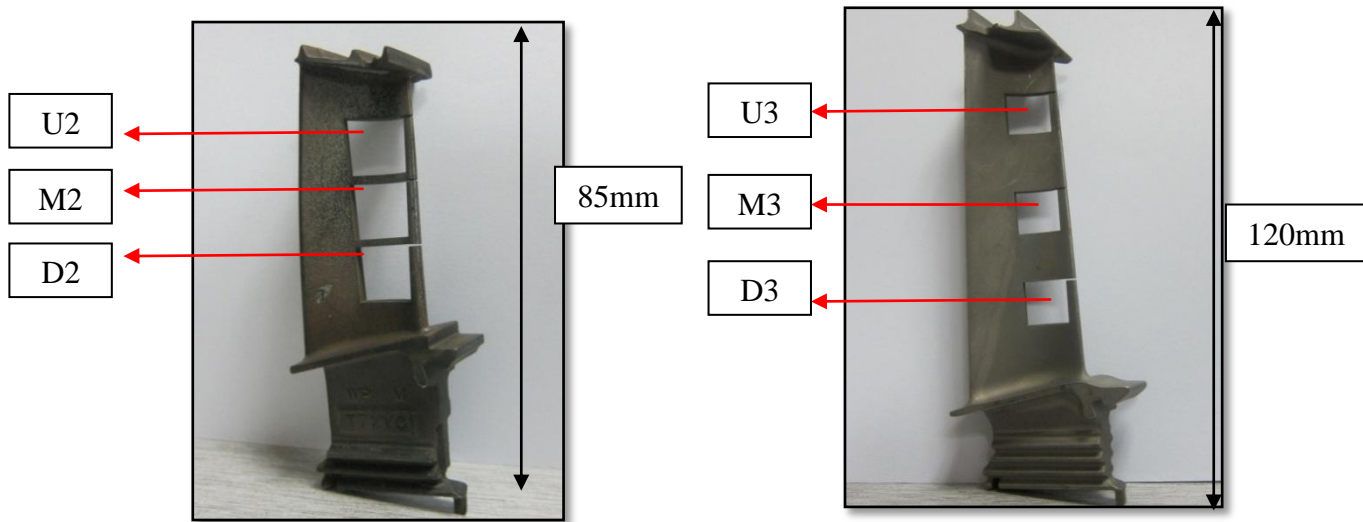


Figure 4.3b: Turbine Blade 2<sup>nd</sup> Stage

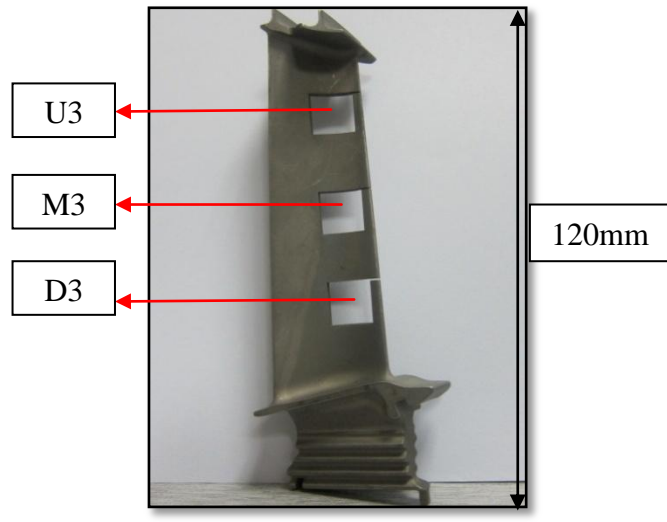


Figure 4.3c: Turbine Blade 3<sup>rd</sup> Stage

Figure 4.3: Sections for each stage of turbine blade.

### 4.3 Chemical Analysis

All specimens were analyzed for chemical analysis (see Table 4.1) to see the variation of element present on each stage. The closest standard material found in the literatures used for comparison. From the analysis, the turbine rotor blades are manufactured from single crystal nickel-base super alloys, SRR99 were developed by Rolls Royce consists of Aluminum, Titanium, Chromium, Cobalt, Nickel and Tungsten [14]. Single crystal turbine blades have the mechanical advantage of being able to operate at a much higher temperature than crystalline turbine blades. This will help to increase turbine efficiency with the ability to withstand higher temperatures due to the single crystal structure and the composition of the nickel based super alloy itself.

The single crystal structure has the ability to withstand creep at higher temperatures than crystalline turbine blades due to the lack of grain boundaries present. The lack of these grain boundaries inhibits creep from occurring, though creep will still occur in single crystal turbine blades but due to different mechanisms at higher temperatures. The single crystal turbine blade does not have grain boundaries along directions of axial stress which crystalline turbine blades do [15]. This also works to increase the creep strength.

*Table 4.1:Material composition for each sample.*

<b>Sample (Wt %)</b>	<b>Journal (Wt %)</b>	<b>UI</b>	<b>D1</b>	<b>U2</b>	<b>M2</b>	<b>D2</b>	<b>U3</b>	<b>M3</b>	<b>D3</b>
O	-	3.81	3.26		1.42	1.36	7.89	11.0	8.13
Al	5.5	6.29	10.1	6.91	4.41	6.69	5.82	5.61	5.57
S	-						0.58	0.69	0.48
Cl	-	0.71					1.07	1.67	0.82
Ti	2.2	0.84	0.9	0.56	0.93	0.68	1.08	0.96	0.82
Cr	8	3.97	2.52	5.3	8.03	5.62	6.96	7.47	6.11
Co	5	6.61	5.10	6.82	8.78	7.86	8.69	8.52	6.92
Ni	-	64.4	65.32	63.6	52.86	62.23	57.61	55.65	56.70
Ta	3	2.81			7.35				3.63
W	10	10.4	10.9	9.62	10.2	9.37	11.7	10.9	10.8
Si	-		1.84		-1.3	0.99			
C	-			7.15	7.34	5.21	-1.42	-2.57	

The superior high temperature behavior of these materials is attributed to the two-phase composite microstructure consisting of a  $\gamma$ -matrix (Ni) containing a large volume fraction of  $\gamma'$ - particles (Ni<sub>3</sub>Al). The  $\gamma'$ - particles phase needs to be greater than 50% volume fraction in the super alloy to provide the increase in creep resistance. The presence of the gamma prime phase increases the mechanical strength of the turbine blade by preventing dislocation motion. The gamma prime phase has the unusual property of increasing strength as temperature increases. This is true up to 973°C.

Cr and Co partition preferentially to the austenitic face centred cubic nickel-based *matrix* where they act mainly as solid solution strengthening elements. Cr plays an essential role in the hot corrosion resistance since it promotes the formation of a protective Cr<sub>2</sub>O<sub>3</sub> oxide scale. From the table, Cr and Co composition were low for turbine blade stage 1 compared to their composition amount in blade at stage 2 and 3. These alloys contain a high volume fraction of strengthening ordered Ni<sub>3</sub>Al-based  $\gamma'$  phase particles homogeneously distributed in the  $\gamma$  matrix as near cubical precipitates [16].

Based on Figure 4.4, Ti amount is in the range between 0.8 to 1.0 wt% and Ta has the highest amount, 7.35wt%. The element Ti and Ta strengthens the  $\gamma'$  precipitates by substituting to Al in Ni<sub>3</sub>Al. Al also plays a fundamental role in promoting the formation of a stable Al<sub>2</sub>O<sub>3</sub> alumina surface scale which protects the alloy against further oxidation. Several elements are added in small quantities for control of grain structure and mechanical properties that are strongly influenced by grain boundaries. Minor additions of C tend to result in the formation of carbides, often located at the grain boundaries.

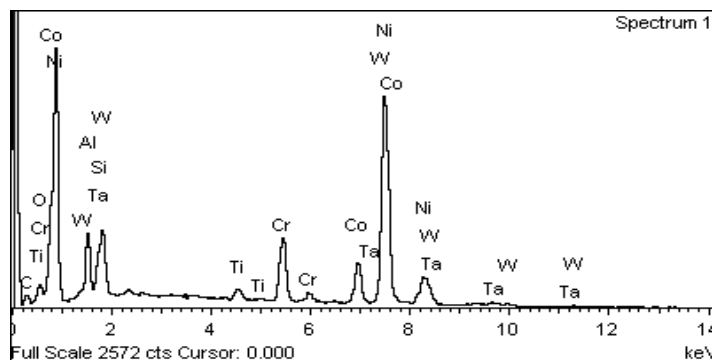


Figure 4.4: Chemical composition for sample M2.

## 4.4 Microstructure Analysis

### 4.4.1 Particle Size Measurement

The analysis will be focusing on the evaluation of the morphology change of the  $\gamma'$  particles size and shape and carbide precipitation for detecting material degradation due to service at high temperature. In general, the  $\gamma'$  precipitates can change in morphology, shape and size during applications resulting in deterioration in high temperature mechanical properties. These microstructural changes often lead to premature failure in gas turbine engines.

The grain size has a significant effect on the material properties, particularly the material strength. Linear Intercept Method and manual calculation was used to calculate the particle diameter of each sample. Equation below was used to calculate the average size of particle.

$$d = \frac{C}{n_L \times m} \quad (1)$$

Table 4.2: Average particle diameter for each sample.

Sample	U1	D1	U2	M2	D2	U3	M3	D3
Grain Diameter ( $\mu\text{m}$ )	1.053	0.882	0.789	0.619	0.690	1.017	0.625	0.480

From Table 4.2, first stage blade, the particle size of sample in first stage blade increase with increase of temperature and proved the temperature distribution in Figure 4.2. First stage blade had been introduced to highest temperature from combustor line in range of 950°C -1057°C. In second stage blade, the grain size increase with increase of temperature, however, the particle size of middle part (M2) slightly smaller than D2. For third stage turbine blade, the particle size increased when the temperature at lower part of turbine blade. The correlation of particle size and temperature will be discussed on the next section.

#### 4.4.2 Correlation of Particle Size and Temperature

By finding the particle size of each sample, a correlation between the effect of temperature on the microstructure of  $\gamma'$  phase has been determined. During prolonged exposure to service temperatures, the shape, size and morphology of the precipitates continuously change. The turbine blade lives are generally dictated by these changes. Increase in temperature and stress accelerates these undesirable changes and thereby, brings down the blade lives significantly. If the temperature exceeds beyond a limit, the  $\gamma'$ -precipitates may completely dissolve leading to sudden deterioration of the high temperature mechanical properties [12].

A relationship between the particle size and temperature of turbine blade SRR99 was constructed referring to the studies been done before. Figure 4.5 show the relationship between aging temperature and gamma prime particle size on the wrought nickel based superalloy [17] and Figure 4.6 shows the relationship between grain size and temperature when strain rate is  $0.01 \text{ s}^{-1}$ , holding time is 30 minutes. Both graphs show that when temperature increases, the particle size will be increased exponentially.

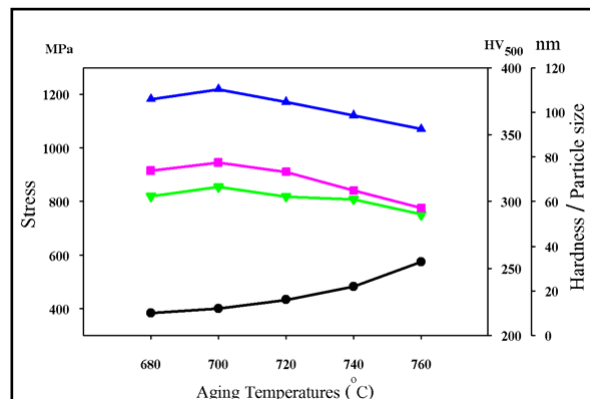
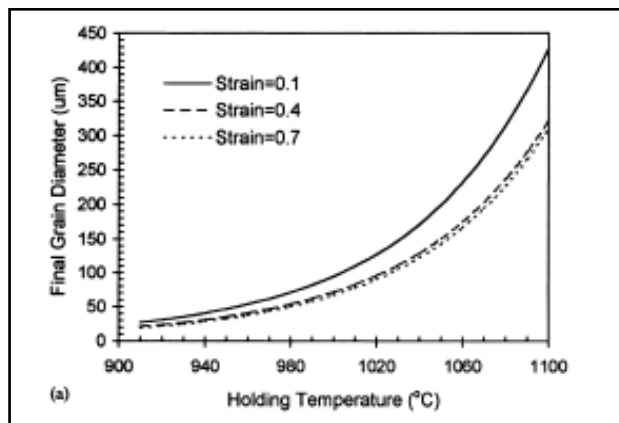


Figure 4.5: The relationship between mechanical properties and gamma prime particle size.

Figure 4.5 also shows that when temperature increased, hardness, yield strength and ultimate tensile strength (UTS) behaviors have the same trend which initially increase with the particle size and then continuously decreased with temperature. It could be noted that all mechanical properties are obviously related to the size of precipitate  $\gamma'$  particles in matrix.

The relationship between particle size and temperature can also be predicted on the previous work [18] as shown in Figure 4.6. From this work, the final grain size of IN718 is related to the holding and deformation temperature and also strain and strain rate prior to the holding period. The higher is the temperature, the larger is the final grain size. At a higher temperature, a dynamically recrystallized grain grows more easily than that at a lower temperature during a hot deformation process because atoms diffuse and move more easily.



*Figure 4.6: The relationship between grain size and temperature when strain rate is  $0.01\text{ s}^{-1}$ , holding time is 30 min.*

Both graphs show that the particle size exponentially increased with temperature. Therefore, the particle size of each sample of blade was plotted on the graph exponentially with respect to the graph found in the literature. A comparison of grain size and temperature were performed to see the relationship between them.

Results were tabulated in Table 4.3. In this table, the temperatures of each blade were estimated first according to the initial value of temperature come from combustor part which is 950 – 1057 °C. Graph in Figure 4.7 were extrapolated exponentially until the maximum temperature and maximum grain size. The maximum of grain size were estimated from previous work [19], the microstructure periodicity also depends strongly on the temperature, showing values from 750–1450 nm. The grain size calculated before (refer Table 4.2) were plotted on the trend line to obtain the temperature value.

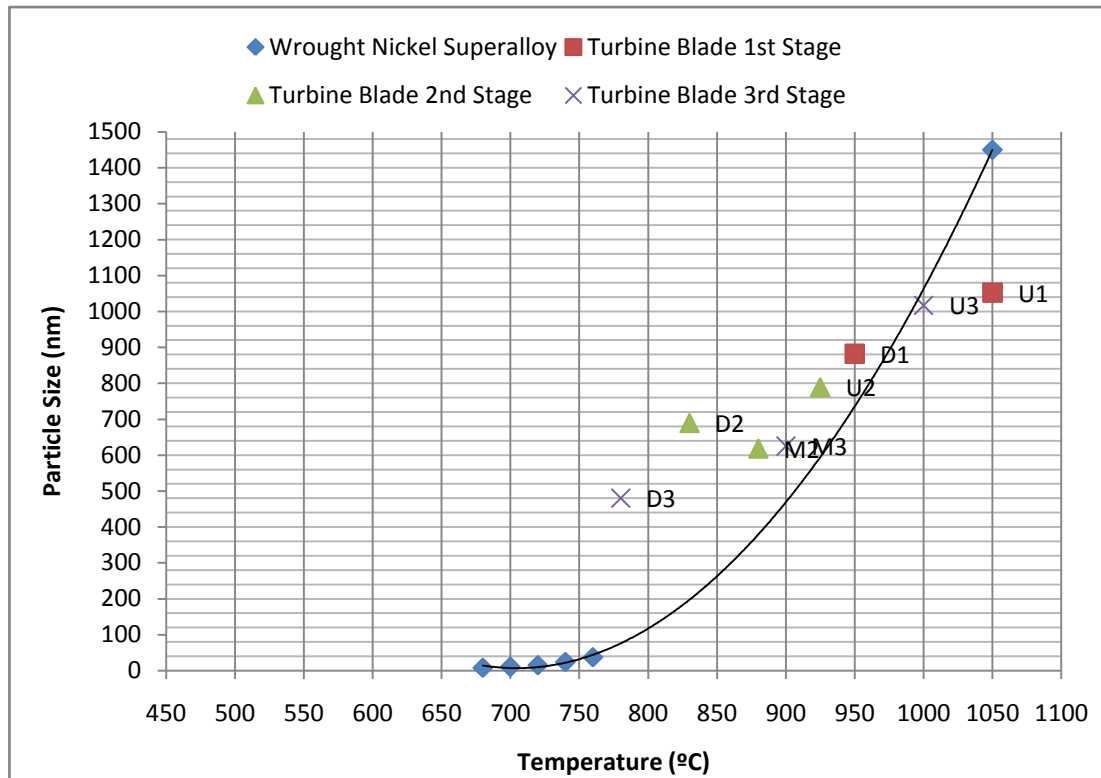


Figure 4.7: Relationship of particle size of gas turbine blade and temperature.

From these graph and table, the temperature faced by the turbine blade at each sample can be estimated.

Table 4.3: Temperature estimation from particle size of gas turbine blade.

Sample	U1	D1	U2	M2	D2	U3	M3	D3
Particle Size (nm)	1052.63	882.35	789.47	618.56	689.66	1016.95	625.00	480.00
Temperature								
Estimation (°C)	1050	950	925	880	830	1000	900	780
Graph Trend line (°C)	1000	975	958	928	942	994	930	902

In first stage blade, the temperature increase with increase of grain size. The temperature in U1 is higher than temperature in D1. In U1, the material was exposed to temperature of 1000°C, almost the same with the highest operating temperature introduced to the blade from combustor chamber. The temperature drops by 25°C from higher part to lower part of blade.

The graph shows that for second stage blade, temperature also drops from higher part to lower part. However, the temperature in the middle section smaller than in the lower section. The temperature of second stage blade was in the range between 920°C to 960°C.

The relationship between particle size of microstructure and temperature can also be seen in third stage turbine blade. With the increment of particle size, the temperature also increased. U3 show that at particle size 1016.95nm, the temperature was the highest at 994°C. Meanwhile at D3, the lowest section, the particle size was 480nm at temperature of 902°C. Therefore, we can that the temperature increased from lower section to middle section and then to upper section.

The correlation between temperature and microstructure on every stage of turbine blade can also be performed. From Figure 4.8, an increment on particle size can be seen when the temperature are higher at upper part (U1, U2 and U3) of turbine blade. The particle size was smaller when the temperature drops from 1<sup>st</sup> stage blade to 3<sup>rd</sup> stage blade. This relationship also is applied on the middle and lower section on the blade. At lower section (D1, D2 and D3, the temperature drop from 975°C to 902°C. At D1, the microstructures were fully rafted with angular shape while the microstructures in D3 were very fine and in cuboidal  $\gamma'$  shape. The evolution of particle size and shape can be concluded due to high temperature and stress applied from turbine.

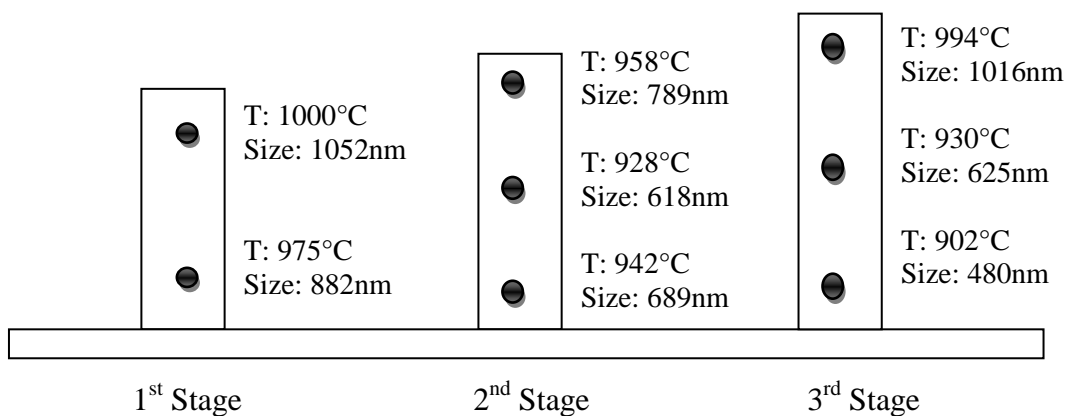


Figure 4.8: Temperature and particle size relationship on the blade arrangement.

### 4.4.3 Microstructure Degradation

During high temperature loading, the regular microstructure of nickel-base superalloys consisting of a  $\gamma$ -matrix (Ni) containing a large volume fraction of  $\gamma'$ -particles (Ni<sub>3</sub>Al) degrades. The strengthening effect of the  $\gamma'$ -precipitates depends largely on their size and morphology. The cubic precipitates coarsen and elongate in a direction normal to the applied stress in a process called rafting. It is very important to study on the effect of rafting to the sample of gas turbine internal blade. According to (Tinga, 2009), the whole range of revealed microstructures can be sorted into four classes which depend on the particle size and temperature been exposed. This category will be explained according to the blade section on every stage.

- First Stage Blade

Significant changes occurred in the microstructure of the base alloy of first stage blade during service aging 24000 hrs at the highest operating temperature, 950 °C - 1050 °C hot gas coming from combustor part. The blade was subjected to hot gas temperature from combustor to first stage vane. Figure 4.9a show a rafted  $\gamma'$  resulting from exposure to stress at high temperature.

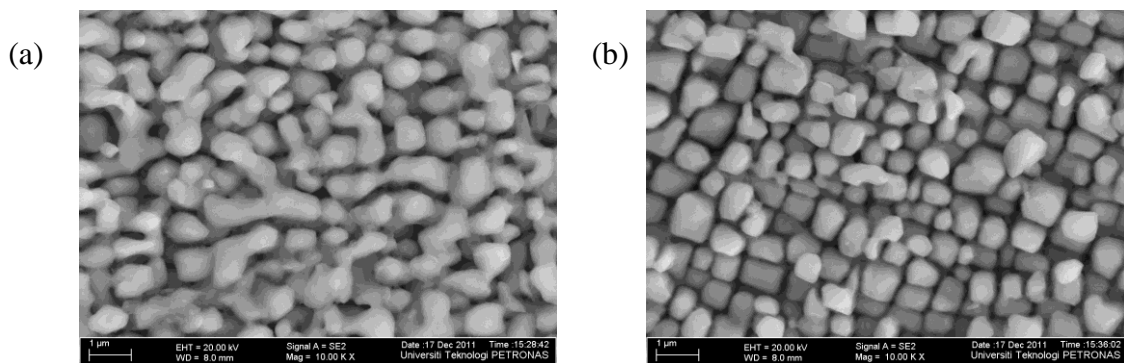


Figure 4.9:  $\gamma'$  morphology (a) rafted particle size  $1.053\mu\text{m}$  for sample U1 and (b) with particle size  $0.882\mu\text{m}$  for sample D1.

The grain size of sample U1 increase due to the high temperature compared to sample D1. The initial  $\gamma'$ -cuboidal particles shape transform into plates shape when temperature increased. Here, it is prove that alongside the blade, the temperature will

be increase from lower part to upper part and the increment is around 1000°C - 1100°C (refer Table 4.3). The blade is also subjected to constant load of gas turbine.

During high temperature service ( $T > 925$  °C), the microstructure gradually degrades by a coarsening process. In the presence of stress, caused by the centrifugal load in a gas turbine blade, a severe directional coarsening, so-called rafting, of the initially cuboidal  $\gamma'$ -particles into a plate-like structure occurs as shown in Figure 4.9a. Spontaneous rafting is observed experimentally at high temperatures and is attributed to internal stresses (e.g. misfit stress, dislocation induced back stress or dendritic stress) that act as a driving force for rafting. The precipitate volume fraction remains more or less constant during rafting at temperatures below 980 °C.

From numerous experimental and theoretical investigations, the driving force for rafting is the combination of the external and misfit stress into a hydrostatic stress that affects the chemical potential of the atoms resulting in diffusion [20]. Further, plastic deformation causes a loss of coherency and reduction of the misfit, which enables rafting. Comprehensive review on rafting by Nabarro and Sujata, Madan, Raghavendra, Venkataswamy & Bhaumik summarize that preferential coarsening of cuboidal  $\gamma'$ -precipitates occurs perpendicular to the applied stress under tension, while they tend to grow parallel to the applied stress under compressive loading. Creep damage to superalloy blades is unavoidable. However, again, one of the criteria for assigning the blade lives is based on the extent of creep damage that is expected for given engine operational conditions, i.e., temperatures and stresses.

Both microstructure on Sample U1 and D1 (shown in Figure 4.9a and 4.9b) been introduced to temperature above 925°C. The materials show a much faster degradation. As a result, the microstructure is fully rafted and considerably coarsened. Microstructure of U1 have been exposed to higher temperature, therefore, the  $\gamma'$  phase is more rafted compared to D1 under 24 000 operating hours. Microstructure in D1 is still in angular shape though the rafting already initiated by the high temperature (975°C) and high stress.

During service, the single crystal nickel based superalloy components also subjected to biaxial state of stress in some regions. These stresses are generated due to (i) the

thermal gradients in cooled regions, (ii) bending stresses exerted by the flowing gas on the blade and (iii) local stress concentrations. In these circumstances, rafting in real components occurs under a multiaxial state of stress and creep test can be performed to study the influence of this stress on  $\gamma'$  rafting. [10]

- Second Stage Blade

The degree of degradation, as evaluated by the gamma prime particle size, increases with exposed time and service temperature. The primary gamma prime particle size varied from 0.789  $\mu\text{m}$ , 0.619  $\mu\text{m}$  to 0.69  $\mu\text{m}$ , as shown in Figure 4.10. The microstructure shows significant degradation in service. The primary gamma prime particles have been spheroidized and secondary gamma prime coarsened in the sample [21]. From the reducing  $\gamma'$  volume fraction and increasing size of particle size, it can be concluded the temperature increased alongside the blade from lower part to upper part.

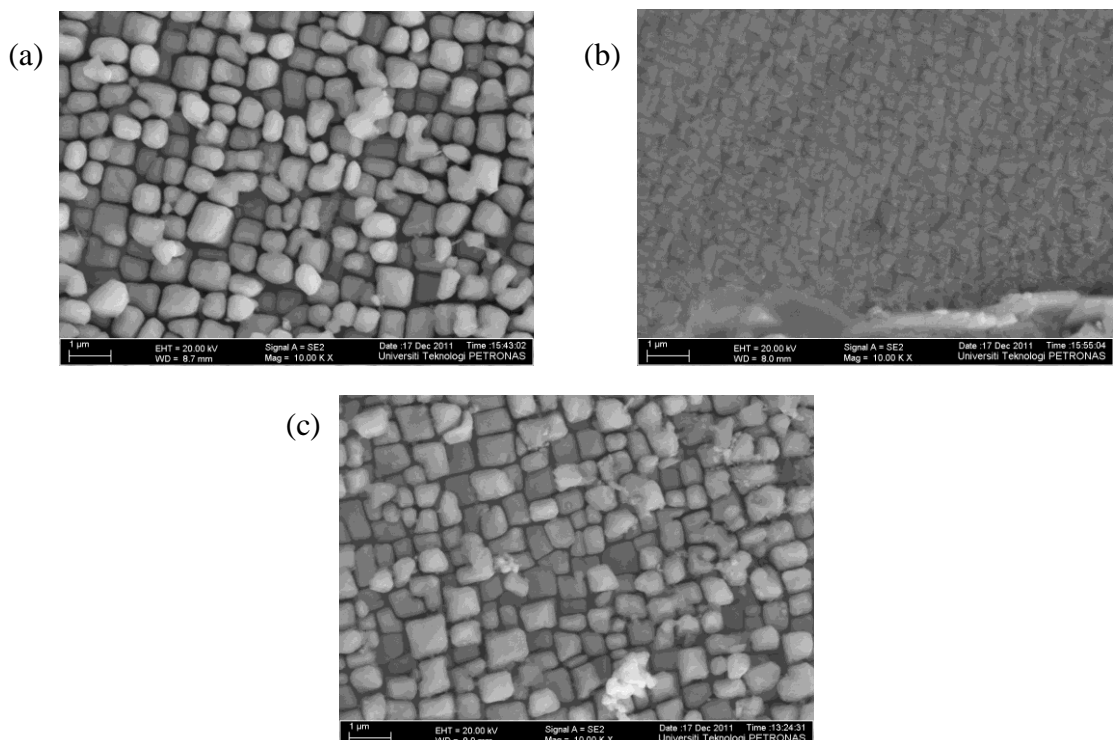


*Figure 4.10:  $\gamma'$  morphology (a) of particle size 0.789  $\mu\text{m}$  for sample U2 and (b) of particle size 0.619  $\mu\text{m}$  for sample M2 and (c) of particle size 0.69  $\mu\text{m}$  for sample D2.*

The blade was subjected to hot gas temperature from first stage blade at around 940 - 960 °C. Initially, both  $\gamma$  and  $\gamma'$  phases are cubic, with their cube axes parallel; structure extremely fine in scale ( $\gamma'$  cuboids  $<0.5\mu\text{m}$ ). It can be seen that an undamaged structure of  $\gamma'$  quasi cuboids has grown into a little rafted  $\gamma'$  (angular shape) resulting from exposure to stress at high temperature on sample U2 (refer Figure 4.10a). The  $\gamma'$  microstructure shape of sample D2 also changes, partially rafted and have rounded shape with particle size  $0.69\mu\text{m}$ . Depending on the particle size and shape of the sample, sample U2 been operated at consider high temperatures ( $T \sim 958^\circ\text{C}$ ) and gradually decrease along the turbine blade ( $T \sim 942^\circ\text{C}$ ) . The degradation process is rather slow, resulting in partly rafted microstructures after 24000 hours. This means that none of the matrix channels has disappeared completely.

However, at middle section (M2), the particle size and temperature is not corresponding nicely according to the result in first stage blade. The middle section has lower temperature and smaller particle size compared to  $\gamma'$  phase in D2 (refer Figure 4.8). According to (Tinga, 2009), the fully rafted microstructure at the blade centre was not observed in the simulation for two reasons: the operating hours is much shorter than the 24000 hours and the internal blade cooling yields much lower temperatures in the centre region of the blade, which reduces the degradation rate there. The result also prove by (Sujata, Madan, Raghavendra, Venkataswamy, & Bhaumik, 2008) said that the microstructure near the blade root (D2) shows extensive rafting which is not expected in the cold zone of the blade under the recommended engine operation conditions during the entire technical life. This might due to the engine was over-spiced for a significant time.

- Third Stage Blade

As shown in Figure 4.11, the precipitates  $\gamma'$  morphology which were  $0.48\ \mu\text{m}$  in size (D3) in the form of circle/cubic at third stage blade have coarsened during service aging to  $0.625\ \mu\text{m}$  (M3) and  $1.016\ \mu\text{m}$  (D3) [22]. The blade was subjected to hot gas temperature from second stage blade at around  $900\text{--}1000\text{ }^\circ\text{C}$ .

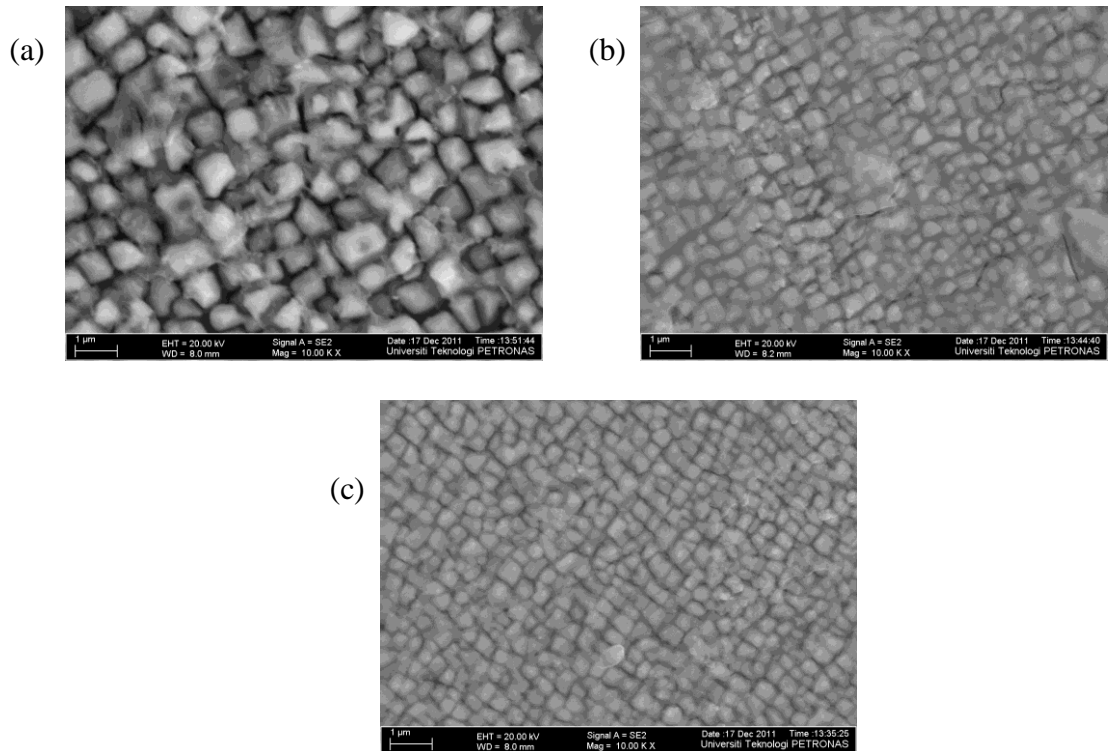


*Figure 4.11:  $\gamma'$  morphology (a) of particle size  $1.016\ \mu\text{m}$  for sample U3 and (b) of particle size  $0.625\ \mu\text{m}$  for sample M3 and (c) of particle size  $0.48\ \mu\text{m}$  for sample D3*

Single crystal nickel based superalloy in U3 had been exposed to highest temperature on the third stage before been removed from turbine package. The particle size and temperature of third stage blade were corresponding to the theory, the higher the temperature, the larger the size of particle. FESEM result of D3 shows that the material were in good condition though been exposed to high temperature ( $902^\circ\text{C}$ ). The  $\gamma'$  still in cuboidal shape with size  $< 0.5\ \mu\text{m}$ .

Material in U3 was subjected to high temperature and high stress. Therefore, the material starts rafted. The microstructure of single crystal superalloys consists of two phases, the ordered intermetallic  $\gamma'$  precipitates coherently embedded in the disordered  $\gamma$  matrix. Under high influence of stress and temperatures  $925^\circ\text{C}$ , the

initially cuboidal  $\gamma'$  precipitates coarsening into extended rafts. The evolution of the microstructure of the single crystal superalloys leads finally to an effect called topological inversion: the  $\gamma'$  phase surrounds the  $\gamma$  phase and becomes topologically the matrix. It has been also shown in several reports that rafting will effect mechanical properties of material such as tensile and creep properties.

Figure 4.11c shows that  $\gamma'$  phase in M3 is isotropically coarsened. According to (Tinga, 2009), the material points experiencing high temperatures, but low stresses and therefore show a more or less isotropic coarsening pattern. This means that the three matrix channels have similar widths, but the microstructure periodicity has increased to values up to 625 nm. This phenomenon is also applied on M2 since the particle size is in between 610 – 660nm. Due to the fact that the present blade is internally cooled, it was subjected to thermal stresses that cause the stress state to be multiaxial.

The degree of service degradation, as measured by the gamma prime particle size, increases with exposed time and service temperature. The coarse gamma prime particle size was approximately 1.052  $\mu$ , while the finest gamma prime particle size was 0.48 $\mu$ m. The relationship between microstructure and exposed temperature of blade can be due to multiaxial degradation which able to correctly simulate the changes in size and shape of the precipitates in the blade. Secondly, the mechanical response of the degraded blade depends on the microstructure morphology in each individual material point. Subsequently, the operating condition of gas turbine also influenced the particle size of the blade. For example, sample D3 were found rafted from this turbine package and the temperature analyzed is very high. At third stage blade, the temperature should be lower than first stage blade. This might due to failure in internal cooling or oversped during operation.

## 4.5 Hardness Testing

Table 4.4: Hardness value for each sample.

Sample	HV	HRC	HV (MPa)	O <sub>y</sub>
UI	465.4	46.5	4564	1141
D1	405.7	41.3	3979	994.75
U2	418.6	42.6	4105	1026.25
M2	417.8	42.5	4097	1024.25
D2	427.8	43.4	4195	1048.75
U3	465.6	46.5	4566	1141.5
M3	598.1	55.1	5866	1466.5
D3	582.5	54.3	5713	1428.25

If HV is expressed in SI units the Yield Stress of the material can be approximated as

$$\sigma_y = \frac{H_V}{c} \approx \frac{H_V}{3} \quad (2)$$

From the hardness value (see Table 4.4), we can see that the constant load and high temperature for 24000h service hours has changed the mechanical properties of the blade. The original yield strength = 1021 MPa. The difference between strength of every sample with the original one is due to change of  $\gamma$  precipitation and also carbide precipitation at grain boundaries. The yield strength increases with increasing temperature from 0 to 850 °C, while it decreases evidently with increasing temperature from 850 to 1050 °C [23]. However, the yield strength of each sample almost does not vary below the peak temperature, 1050°C.

The  $\gamma'$  phase shows an unusual property in that it tends to increase in strength with increasing temperature, at least at lower temperatures below about 800°C. This is significant when the second phase is in excess of 50%, as is often the case with high temperature nickel alloys.

The mechanical behavior of superalloy is closely related to single phase  $\gamma'$ . It should be noted that considerable differences are introduced into mechanical properties of superalloy owing to its two-phase microstructure compared with single phase  $\gamma'$ . For example, single crystal superalloy exhibits highly complex yield behavior. Most single crystal superalloys display a similar peak temperature at which the yield strength achieves a maximum. Above the peak temperature, the yield strength drops rapidly with the increase of temperature. On the contrary, the relationship between yield strength and temperature varies significantly for different alloy below peak temperature [23].

## CHAPTER 5

### CONCLUSION & RECOMMENDATION

The turbine blades operate at elevated temperatures at the very edge of metallurgical alloy development. Three probable damage mechanisms affect turbine blades, these being mechanical damage through either creep or fatigue and high temperature corrosion. Thorough analysis, the microstructure went transformations which likely degrade the mechanical properties of the alloy by  $\gamma'$  coarsening, rafting phenomenon, grain size increment with respect to temperature.

The regular microstructure of nickel-base superalloys consisting of a g-matrix (Ni) containing a large volume fraction of g'-particles (Ni<sub>3</sub>Al) degrades during high temperature and high stress. The cubic precipitates coarsen and elongate in a direction normal to the applied stress in a process called rafting. Due to the transformation of particle size, it is concluded that the temperature blade was increased from lower zone to upper zone. The study also show that the particle size increase from third stage blade to first stage blade. Therefore, the operating temperature of gas turbine in the industry need to be maintain so that the microstructure of blade is not affected and as well reduce the lifespan of turbine blade.

A complete profile or pattern of temperature and particle size was completed. The objectives of this project were successfully achieved. Thus, to improve the study in the future work, unused sample of Nickel based Superalloy can be analyze to compare with the damaged blades. The microstructure of this virgin sample can be used as reference when comparing the particle size and shape. Creep test analysis can also be performed to monitor the mechanical properties of blades with respect to temperature. Heat treatment might also be performed to get better distinction of microstructure transformation of every sample alongside the turbine blade.

---

## REFERENCES

- [1] Ganesan, V. (2006). Gas Turbine. New Delhi: Tata McGraw-Hill Publishing Company Limited.
- [2] Harrison, G., & Henderson, M. (2000). Lifting Strategies for High Temperature Fracture Critical Components. Life Assessment of Hot Section Gas Turbine Components , 11-33.
- [3] Carter, T. J. (2004). Common failures in gas turbine blades. Engineering Failure Analysis, 237-247.
- [4] Naeem, M. T., Seyed, A. J., & Rezamahdi, N. (2008). Failure Analysis of Gas Turbine Blades. 1-16.
- [5] Benes, J. (2008, March). RX for High-Nickel Anxiety. Retrieved August 2011, from Cutting Tool Central: <http://www.cutting-tool.americanmachinist.com/ArticleDraw.aspx?artid=84252>
- [6] Voort, G. F., Manilova, E. P., & Lucas, G. M. (2009). Metallographic Techniques For Superalloys.
- [7] Vardar, N., & Ekerim, A. (2006). Failure analysis of gas turbine blades in a thermal power plant. Engineering Failure Analysis 14 , 743-749.
- [8] Xie, Y.-j., Wang, M.-c., Zhang, G., & Chang, M. (2006). Analysis of superalloy turbine blade tip cracking during service. Engineering Failure Analysis 13 , 1429–1436.
- [ix] Kubiak, J., Urquiza, G., Rodriguez, J., González, G., Rosales, I., Castillo, G., et al. (2009). Failure analysis of the 150MW gas turbine blades. Engineering Failure Analysis .
- [x] Mazur, Z., Luna-Ramirez, A., Juarez-Islas, J., & Campos-Amezcuca, A. (2004). Failure analysis of a gas turbine blade made of Inconel. Engineering Failure Analysis, 474-486.
- [11] (2000). Rolls Royce Allison 501-Kb7 Industrial Engine Operation And Manual.
- [12] Sujata, M., Madan, M., Raghavendra, K., Venkataswamy, M., & Bhaumik, S. (2008). Microstructural Study: An Aid To Determination Of Failure

- 
- Mechanism In Nickel Base Superalloy Blades. Transactions Of The Indian Institute Of Metals , 681-685.
- [13] Ikeguchi, T., Noda, M., & Anzai, S. (1995). Gas Turbine And Gas Turbine Blade.
- [14] Pollock, M. T., & Tin, S. (2006). Nickel-Based Superalloys For Advanced Turbine Engines:Chemistry, Microstructure, And Properties. Journal Of Propulsion And Power , 1-14.
- [15] Das, N. (2008). Advances In Nickel-Based Cast Superalloys. Transactions Of The Indian Institute Of Metals , 265-274.
- [16] Schneibel, J. H. (2008). Beyond Nickel-Base Superalloys. 1-14.
- [17] Lothongkum, G. Khuanlieng, W. Homkrajai, W. & Wangyao P. (2006). Effect Of Pre-Heat Treatments On Nano  $\Gamma'$  Precipitation And Mechanical Properties In Wrought Nickel Base Superalloy, X-750. 7-13.
- [18] Zhang, J., Gao, Z., Zhuang, J., & Zhong, Z. (2000). Grain Growth Model Of In718 During Holding Period After Hot Deformation. Journal Of Materials Processing Technology 101 , 25-30.
- [19] Tinga, T. (2009). Multiscale Modelling of Single Crystal Superalloys for Gas Turbine Blades. Eindhoven.
- [20] Kamaraj, M. (2003). Rafting in single crystal nickel-base superalloys – An Overview. 115-128.
- [21] Wangyao, P., Krongtong, V., Tuengsook, P., Hormkrajai, W., & Panich, N. (2006). The Relationship Between Reheat-Treatment And Hardness Behaviour Of Cast Nickel Superalloy, Gtd-111. Journal Of Materials And Minerals, Vol.16 No.1 , 55-62.
- [22] Kubiak, J., Urquiza, G., Rodriguez, J., González, G., Rosales, I., Castillo, G., et al. (2009). Failure analysis of the 150MW gas turbine blades. Engineering Failure Analysis
- [23] Liu, J.-L., Yu, J.-J., Jin, T., Sun, X.-F., Guan, H.-R., & Hu, Z.-Q. (2010). Influence Of Temperature On Tensile Behavior And Deformation Mechanism Of Re-Containing Single Crystal Superalloy. Transcation Of Non Ferrous Metal , 1518-1523.

## APPENDIX I

Gantt chart and Equipment & Tool Required



### Tool or Equipment Required

No.	Tool / Equipment	Description	Availability
1.	Gas turbine blades	Set of rotors from different stages	Provided by PETRONAS Carigali Sdn Bhd
2.	EDM	To perform the sectioning	Material Lab Building 16
2.	Grinding machine	Refine the surface of turbine blades	Material Lab Building 17
3.	Optical microscopy	Observe the microstructure in the unetched condition first to obtain meaningful images before etching the sample.	Material Lab Building 17
4.	Field Emission Scanning electron microscope (FESEM)	Scanning sample with a high-energy beam of electrons in a raster scan pattern.	Centralized Analytical Lab, Block P
5	Energy dispersive spectroscopy x-ray (EDS)	Used in conjunction with the Field Emission Scanning Electron Microscope (FESEM) providing chemical analysis in areas as small as 1 $\mu\text{m}$ in diameter.	Centralized Analytical Lab, Block P
7.	Micro Hardness Test Machine	Determine the hardness value of various materials including metals, alloys and etc.  Method: Vickers hardness test	Material Lab Building 17

## APPENDIX II

### Operating Parameters Provided by Rolls Royce

## Operating Parameters

Table 2-1 Operating Parameters			
Parameter	*Control Limit Setting (Continuous Operation)	Warning Setting	*Shutdown Setting
Engine Speed (N1)	14,200 to 14,600 rpm	At 15,400 rpm and above	15,800 rpm
Control Temperature (CT)	1935°F (1057°C)	2000°F (1093°C)	2020°F (1104°C) for 10 sec or 2070°F (1132°C) for 100 milliseconds**
Fuel flow (W <sub>f</sub> )			Fuel valve mistrack more than 0.5 v for 1.0 sec

\*These are maximum settings established by Rolls-Royce Corporation. The OEM may have established lower settings, but cannot exceed the Rolls-Royce Corporation maximum settings for particular units.  
\*\*Maximum time period is 10 seconds (Ref. Table 2-2)

## Operating Limits

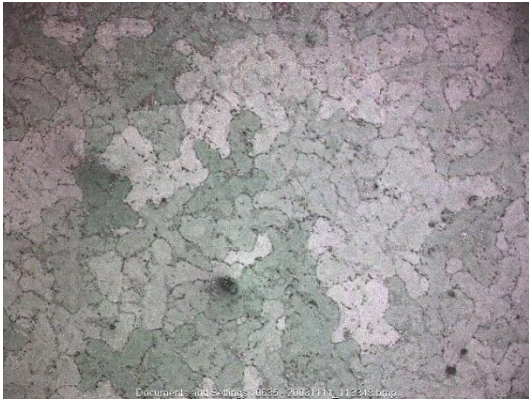
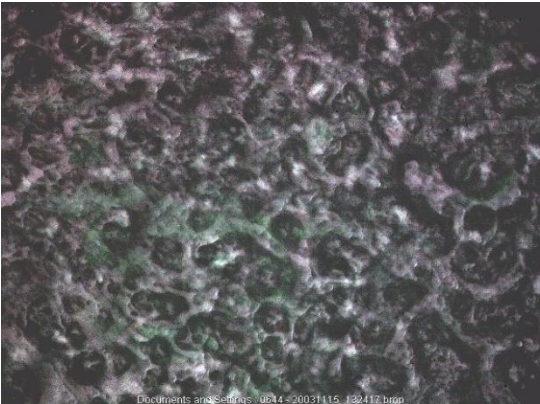
Table 2-2 Operating Limits					
	Control Temperature °F (°C)	N1 Engine Speed (rpm)	Oil Pressure psig (kPag)	Oil Temperature °F (°C)	Vibration in./sec (mm/sec)
Starting – Normal	<1570 (854)			–40 to 160 (–40 to 71)	
Starting – Warning	>1570 (854)				
Starting – Shutdown	>1600 (871) <600 (316) within 3 sec and N1 >7200 rpm.  See Note 1.	<7200 within 30 sec. N1 does not accelerate >40 rpm/sec for 3 sec when CT >600 (316) and N1 <13,000.			
Operating – Normal	<1935 (1057)	14,200 – 14,800	50 – 60 (345 – 414)	<160 (71)	
Operating – Warning	>2000 (1093)	>15,400	<40 (276)		
Operating – Shutdown	>2020 (1104) for 10 sec or >2070 (1132) for 100 msec  See Note 2.	>15,800 or <13,000 after speed has been >13,000 for 3 sec.	<20 (138)	>180 (82)	>3 mils (0.07) for 3 sec.

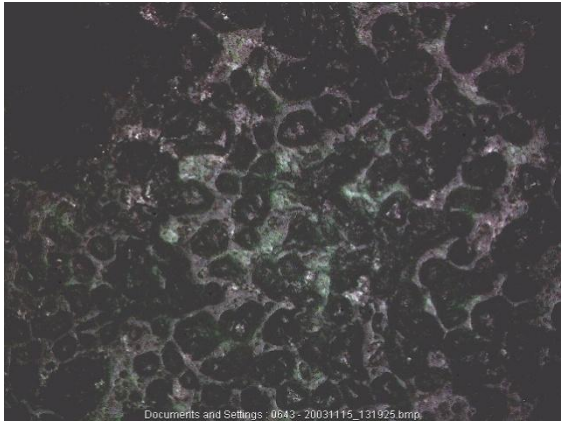
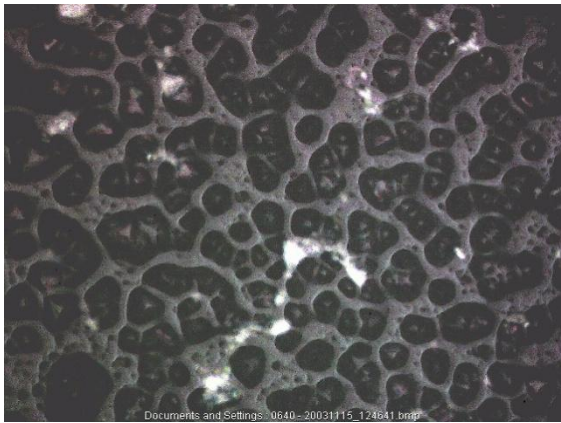
Notes:  
1. Turbine outlet temperature (TOT) over-temperature backup is >1400°F (760°C) and N1 is <13,000 rpm.  
2. TOT run-over temperature backup when N1 is >13,000 rpm.  
3. The symbol > means more than and the symbol < means less than.

## APPENDIX III

### Microstructure Image under Optical Microscope

Image of Microstructure after Etching under Optical Microscope

No	Image	Description
1		<p>Sample : U3</p> <p>Microstructure of SRR99 with a fine grain size, considerable delta and large primary MC carbides revealed using glyceresia.</p>
2		<p>Sample : U1</p> <p>Sample were etched using 50 ml HCl and 1 - 2 ml H2O2 (30%) to attack <math>\gamma'</math> in Ni-base alloys. The sample was immersed for 10 - 15 seconds. No clear image captured due to improper etching.</p>
3		<p>Sample: U3</p> <p>Microscope image of nickel superalloy with smaller grain boundaries by using Marble Reagent. This region was exposed to high temperature of hot gas.</p>

4	 <p style="font-size: small; text-align: center;">Documents and Settings\0643-20031115_131925.bmp</p>	<p>Sample : M3</p> <p>Microscope image of nickel superalloy with bigger grain boundaries than Sample-U3 by using Marble Reagent. This region was exposed to high temperature of hot gas but was cooled down from cooling air.</p>
5	 <p style="font-size: small; text-align: center;">Documents and Settings\0640-20031115_174641.bmp</p>	<p>Sample : D3</p> <p>Microscope image of nickel superalloy with bigger grain boundaries than Sample-U3 and Sample-M3 by using Marble Reagent. This region which is the trailing edge was exposed to high temperature of hot gas but was cooled down from cooling air.</p>

APPENDIX IV  
Chemical Analysis

## Chemical Composition of Ni based Superalloy

**Table I.** Chemical compositions (wt.%) of first generation Ni-based superalloys for single crystal blades.

Alloy	Cr	Co	Mo	W	Al	Ti	Ta	Nb	V	Hf	Density (g.cm <sup>-3</sup> )	Country	Ref.
Nasair 100	9	–	1	10.5	5.75	1.2	3.3	–	–	–	8.54	USA	[37]
CMSX-2	8	4.6	0.6	8	5.6	1	6	–	–	–	8.60	USA	[21]
CMSX-3	8	4.6	0.6	8	5.6	1	6	–	–	0.1	8.60	USA	[21]
CMSX-6	9.8	5	3	–	4.8	4.7	2	–	–	0.1	7.98	USA	[41]
PWA 1480	10	5	–	4	5	1.5	12	–	–	–	8.70	USA	[20]
SRR 99	8	5	–	10	5.5	2.2	3	–	–	–	8.56	GB	[18]
RR 2000	10	15	3	–	5.5	4	–	–	1	–	7.87	GB	[18]
René N4	9	8	2	6	3.7	4.2	4	0.5	–	–	8.56	USA	[33,42]
AM1	7.8	6.5	2	5.7	5.2	1.1	7.9	–	–	–	8.60	F	[12]
AM3	8	5.5	2.25	5	6	2	3.5	–	–	–	8.25	F	[24]

Spectrum processing :

No peaks omitted

Processing option : All elements analyzed (Normalised)

Number of iterations = 3

Standard :

C CaCO3 1-Jun-1999 12:00 AM

Al Al2O3 1-Jun-1999 12:00 AM

Ti Ti 1-Jun-1999 12:00 AM

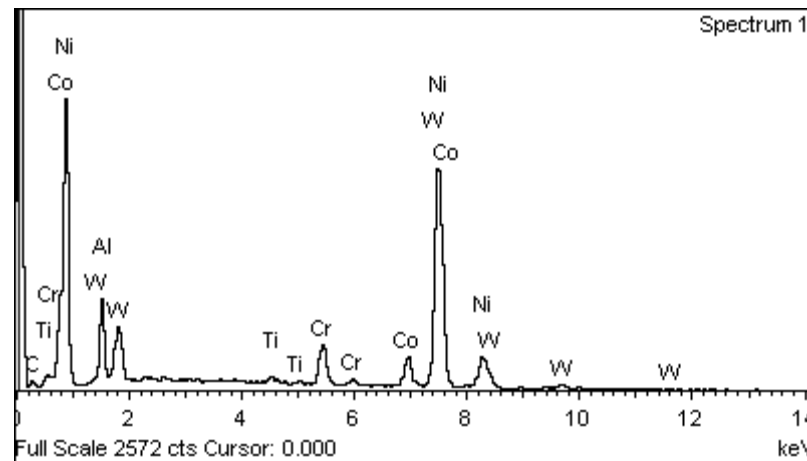
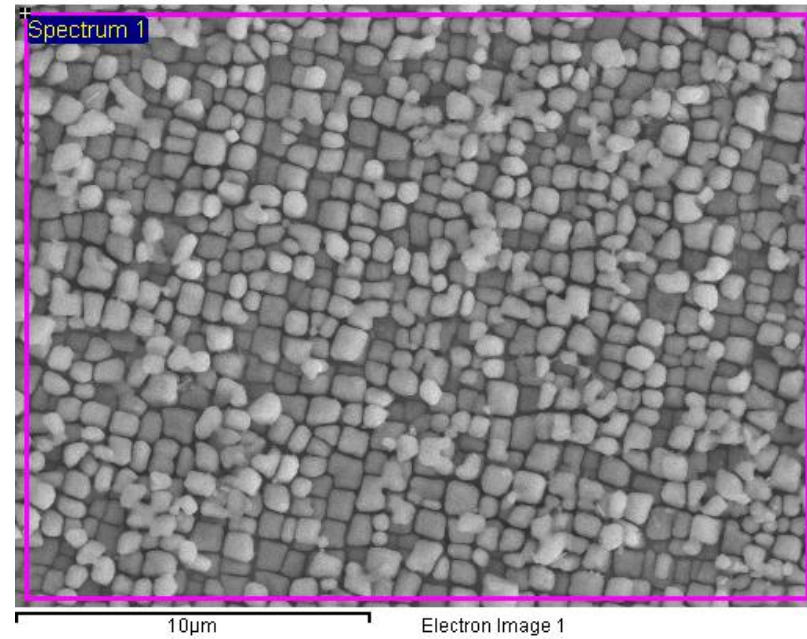
Cr Cr 1-Jun-1999 12:00 AM

Co Co 1-Jun-1999 12:00 AM

Ni Ni 1-Jun-1999 12:00 AM

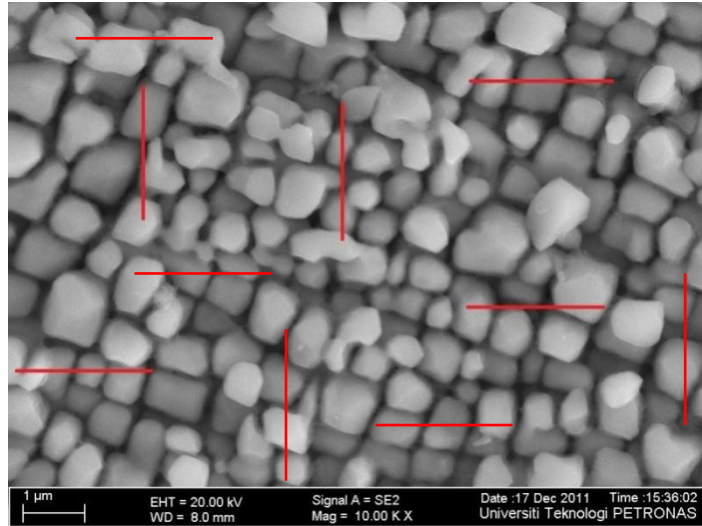
W W 1-Jun-1999 12:00 AM

Element	Weight%	Atomic%
C K	7.15	26.85
Al K	6.91	11.56
Ti K	0.56	0.53
Cr K	5.30	4.60
Co K	6.82	5.22
Ni K	63.63	48.88
W M	9.62	2.36
Totals	100.00	



APPENDIX V  
Sample Calculation for Determining Size

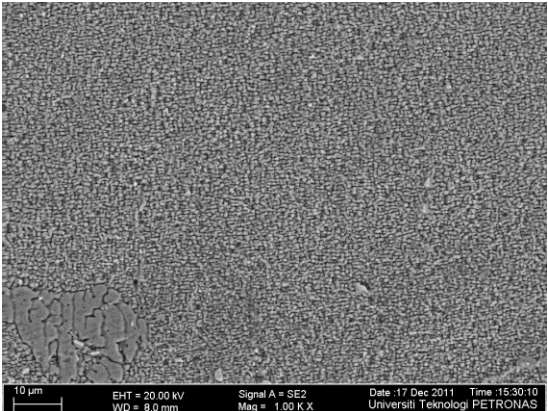
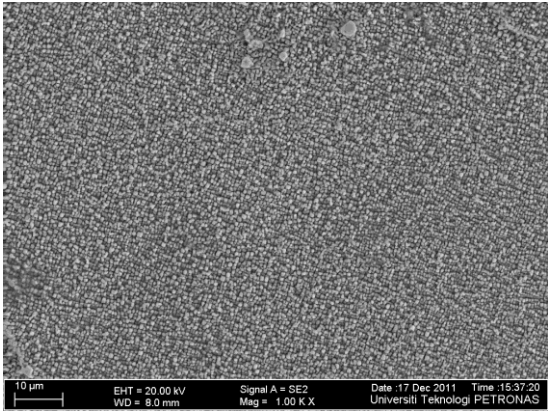
## Linear Intercept Method



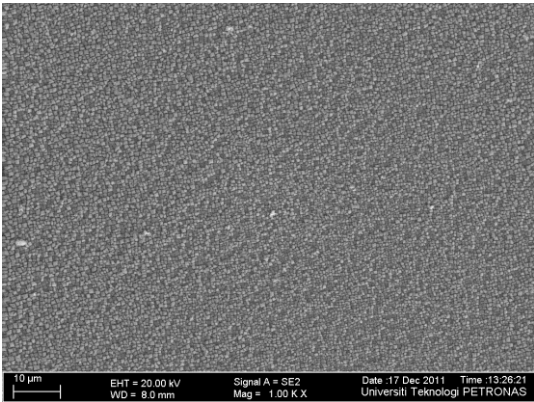
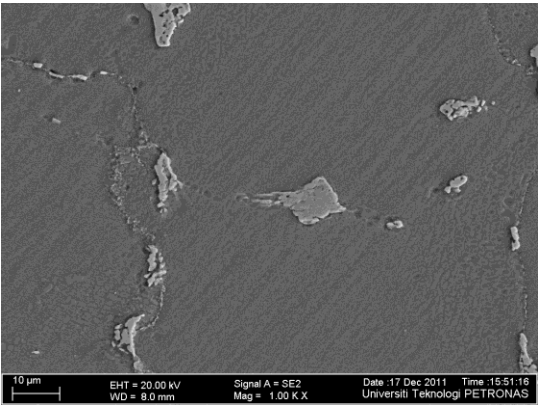
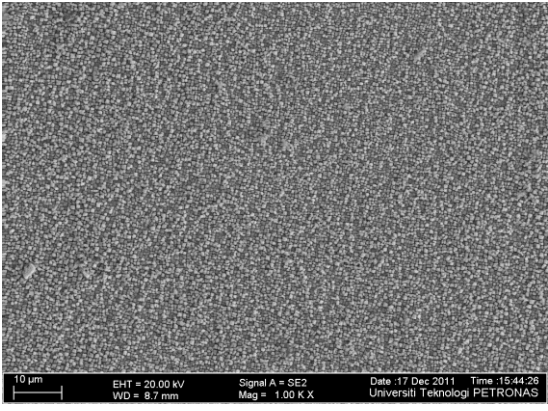
Sample	U1	D1	U2	M2	D2	U3	M3	D3
Line								
1	6	7	8	10	7	5	12	13
2	5	6	8	11	10	6	9	14
3	6	6	7	12	8	6	10	13
4	6	7	7	10	9	5	9	11
5	6	7	8	8	8	5	10	13
6	7	7	6	9	10	7	10	12
7	5	8	8	10	10	7	8	12
8	5	6	8	10	9	6	9	12
9	5	5	8	9	8	6	10	13
10	6	9	8	8	8	6	9	12
Average	5.7	6.8	7.6	9.7	8.7	5.9	9.6	12.5
Line length (mm)	50	50	50	50	50	50	50	50
Grains/cm, $n_L$	0.114	0.136	0.152	0.194	0.174	0.118	0.192	0.25
Magnification, m	12500	12500	12500	12500	12500	12500	12500	12500
Constant, C	1.5	1.5	1.5	1.5	1.5	1.5	1.5	1.5
Grain Diameter (mm)	0.001	0.001	0.001	0.001	0.001	0.001	0.001	0.000
Grain Diameter ( $\mu\text{m}$ )	1.053	0.882	0.789	0.619	0.690	1.017	0.625	0.480

APPENDIX VI  
Microstructure Image at 1000 X Magnification

First Stage Blade



Second Stage Blade



Third Stage Blade

